Materials Horizons

ROYAL SOCIETY OF CHEMISTRY

REVIEW

View Article Online
View Journal | View Issue

Cite this: *Mater. Horiz.*, 2023, **10**, 1924

Chiral-induced spin selectivity in biomolecules, hybrid organic–inorganic perovskites and inorganic materials: a comprehensive review on recent progress

Yingdan Xu and Wenbo Mi *

The two spin states of electrons are degenerate in nonmagnetic materials. The chiral-induced spin selectivity (CISS) effect provides a new strategy for manipulating electron's spin and a deeper understanding of spin selective processes in organisms. Here, we summarize the important discoveries and recent experiments performed during the development of the CISS effect, analyze the spin polarized transport in various types of materials and discuss the mechanisms, theoretical calculations, experimental techniques and biological significance of the CISS effect. The first part of this review concisely presents a general overview of the discoveries and importance of the CISS effect, laws and underlying mechanisms of which are discussed in the next section, where several classical experimental methods for detecting the CISS effect are also introduced. Based on the organic and inorganic properties of materials, the CISS effect of organic biomolecules, hybrid organic–inorganic perovskites and inorganic materials are reviewed in the third, fourth and fifth sections, especially the chiral transfer mechanism of hybrid materials and the relationship between the CISS effect and life science. In addition, conclusions and prospective future of the CISS effect are outlined at the end, where the development and applications of the CISS effect in spintronics are directly described, which is helpful for designing promising chiral spintronic devices and understanding the natural status of chirality from a new perspective.

Received 6th January 2023,
Accepted 14th March 2023

DOI: 10.1039/d3mh00024a

rsc.li/materials-horizons

New concepts

The chiral-induced spin selectivity (CISS) effect has not only revolutionized spintronic devices, but also motivated a new round of exploration of life and Earth. The interactions between electron spin, magnetic field and polarized light show the spin filtering ability of chiral biological systems, making the CISS effect an attractive wider research topic. In this review, the key developments of spin polarized transport in various chiral materials are summarized, where the mechanisms and experimental measurement techniques of the CISS effect are also discussed. More importantly, the biological significance of the CISS effect and the mechanisms of chirality transfer between chiral organic molecules and inorganic frameworks are described in this review, which is helpful for the exploration of life science and the preparation of hybrid organic–inorganic materials. In the future, the CISS effect will become the key to breakthroughs in bioscience and spintronics. Ten potential research contents on the CISS effect are proposed in this review, which involves chiral spiral magnets, chiral composite materials, chiral topological materials and so on. The insight gained from this review will provide help for the research of mechanisms and device applications related to the CISS effect, which will also make the outlook for chiral functional materials clearer.

1. Introduction

Using electron spin as a medium for logical operation has revolutionized the electronic technology and information storage.[1] It is commonly believed that spin-based applications and devices are associated with magnetic materials.[2] However, due to weak spin–orbit coupling (SOC) and hyperfine interaction, the spin relaxation time of organic molecules is longer, which is conductive to the transport of spin polarized carriers. In the past two decades, organic molecules have been widely studied as spin transport media.[3–5] In 1984, Mason first realized the connection between spin and chirality, and found that the weak interaction difference between electrons with opposite spin states led to different ground states of chiral

Tianjin Key Laboratory of Low Dimensional Materials Physics and Preparation Technology, School of Science, Tianjin University, Tianjin 300354, China. E-mail: miwenbo@tju.edu.cn

enantiomers.[6] In 1994, Wang *et al.*[7,8] proposed that 'left-handed (right-handed)' electrons generated by SOC accounted for the majority in right-handed (left-handed) molecules. Based on the electronic transmission in chiral stearyl lysine, the chiral-induced spin selectivity (CISS) effect was proposed by Naaman's group at an experimental level in 1999, which describes the phenomenon that chiral materials with broken inversion symmetry tend to transport electrons in one spin direction and block the other.[9] Since then, a lot of chiral organic molecules[10–14] have been demonstrated to be spin filters, where the efficiency of electron transport depends on the spin direction.

Due to the effective magnetic field generated by the coupling of electron velocity and chiral potential, the degeneracy of spin energy levels in chiral molecules is broken.[15] When electrons move in a chiral potential field, their spin direction tends to be parallel or antiparallel to the velocity.[15] The discovery of the CISS effect provides a new strategy for manipulating electron's spin through organic materials.[16,17] Based on scanning tunnel energy spectra, Alpern *et al.*[18] found the unconventional superconductivity on the surface of Nb film adsorbed chiral helical molecules, paving a way for the application of chiral spintronic devices in the field of superconductivity. The successful application of polyalanine molecules in silicon-compatible nanomagnetic memory devices at room temperature has increased the ratio of 0 (high-resistance) to 1 (low-resistance states) to 3 : 1, making it viable to fabricate nanoscale memory devices.[19] The adsorption layer composed of chiral polymethyl methacrylate can be used as a switch for the magnetization of Co, reducing the current density for reversing magnetization to 10^{13} electrons per square centimeter, which promotes the performance improvement of modern magnetic random access memory.[20]

The ubiquity of chiral molecules indicates their importance in living systems. Spin dependent electron transport properties can be manipulated by applying both polarized light and magnetic fields.[21–24] For example, circularly polarized light induced efficient magnetization by spin torque transfer through a hybrid of quantum dots (QDs) and chiral monolayers, which changes the direction of magnetization of Ni films and exhibits a difference of 5% between the magnetization results of opposite helical circularly polarized light.[25] Charge transfer in chiral oligopeptide hybrid CdSe nanoparticles can be regulated by adjusting the magnetization direction of a ferromagnet, where light serves as a switch of spin channels.[26] The spin filtering ability of the D96N mutant of bacteriorhodopsin (bR) was markedly weakened under light illumination, providing the evidence for light-regulated spin polarization (SP) in living organisms.[27] Thus, the interactions between light, spin, chirality and magnetic fields are the key to breakthroughs in life sciences and spintronic devices. However, systematic analysis of these interactions in life processes has rarely been reported from the perspective of chirality and spin. In recent years, chiral hybrid organic inorganic perovskites (HOIPs) have attracted much attention in spintronics due to the strong SOC and spin dependent chiral optical characteristics.[28–31] The enantiomers of chiral HOIPs exhibit different absorption characteristics for circularly polarized light, which can be adjusted by using organic or inorganic components.[28] Traditional research studies on chiral HOIPs mainly focus on the photovoltaic properties and applications in solar cells,[32] while recent experimental results[33,34] indicate that chiral HOIPs also exhibit spin dependent charge transport mediated by the CISS effect. The combination of chiral molecules and $FASnI_3$ promotes the formation of layered structures and facilitates hole transportation, which increases the power conversion efficiency of solar cells to 10.73%.[35] Inorganic materials are widely used in daily life because of their characteristics of hardness, high temperature resistance and corrosion resistance, where the CISS effect has been confirmed in chiral crystals, nanoparticles and oxides.[36] Under heat induction, the electromagnetic characteristics of inorganic VO_2 based

Yingdan Xu

Yingdan Xu was born in Hebei Province, China, in 1999. She received her BS degree in Applied Physics from the School of Science at Tianjin University, China, in 2021. She is presently a postgraduate student under the supervision of Prof. Wenbo Mi in Tianjin University, China. Her research interests mainly focus on the spin-related physical properties of chiral materials.

Wenbo Mi

Prof. Wenbo Mi received his BS, MS and PhD degrees in Department of Physics from Tianjin University in 2001, 2004 and 2006, respectively. Then he became an assistant professor at Department of Physics, Tianjin University and was promoted as full Professor from 2013. He was the visiting scholar in 2008 at the Hong Kong University of Science and Technology, then he became a Postdoc Fellow in King Abdullah University of Science and Technology in 2010. His research interests mainly focus on the theoretical design, fabrication and physical properties of the low-dimensional spintronic materials.

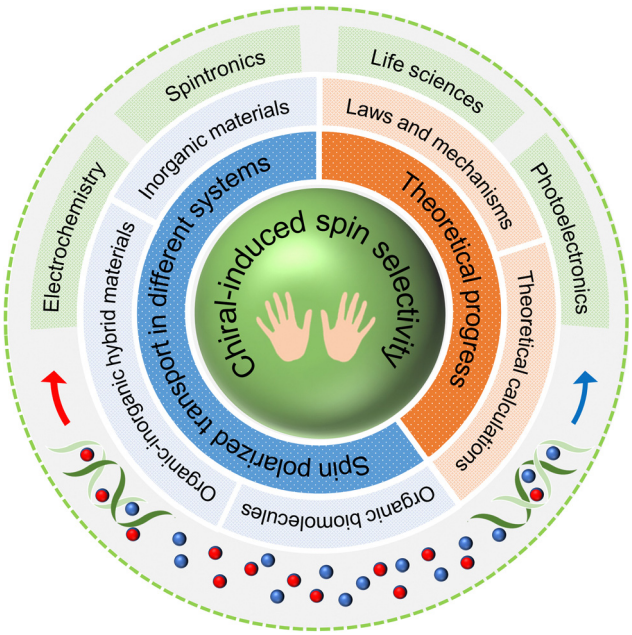

Fig. 1 Schematic diagram for the progress of spin polarized transport processes and theories related to the CISS effect. The CISS effect provides a new idea to manipulate electron's spin, which has important applications in life science, spintronics, electrochemistry and optoelectronics.

chiral metamaterials change from insulator to metal, the slow light effect of which is of great significance to control light polarization.[37]

The spin polarized transport properties of chiral organic biomolecules, hybrid organic inorganic materials and inorganic materials are systematically reviewed in this work, where the theoretical mechanisms and experimental techniques of CISS are also summarized. Effects of influencing factors, such as light, chirality, magnetic field and voltage, on spin polarized transport processes are discussed, especially in life-related processes. In addition, the most straightforward statements regarding the development prospects and potential research contents of the CISS effect are presented, which are conducive to exploring life science, breaking through the magnetic storage technology limitations and promoting the manufacture of high-density spintronic devices (Fig. 1).

2. Chiral-induced spin selectivity effect

2.1. Laws and mechanism

The word 'chiral' is derived from a Greek word and describes the property of asymmetry, that is, one enantiomer can be converted to the other by a mirror symmetry operation. Suppose that A, B, C and D are four different groups connected to a central carbon (C) atom, which are arranged as A > B > C > D from the largest to the smallest group. When the smallest D group is placed at the farthest position in the vision, the other three groups facing the observer can be ranked from large to small, according to which the clockwise (CW) configuration is called Rectus (R) and the counterclockwise (CCW) one is called Sinister (S). Chiral structures couple electron's spin direction and velocity. The CISS effect describes the tendency of chiral materials to transport electrons with one spin direction while blocking those with the other, which endows chiral molecules with the ability of spin filtering.[38] SP is defined as

$$\mathrm{SP} = \frac{I_+ - I_-}{I_+ + I_-} \quad (1)$$

where I_+ and I_- usually represent the theoretical electron intensity, the spin direction of which is parallel and antiparallel to velocity. Experimentally, I_+ and I_- can be concretized into other physical quantities, such as the Faradaic current at specific bias voltage under 'up' and 'down' magnetic field. According to the reported spin transport processes related to the CISS effect, when electrons move through a chiral potential, the spin direction tends to be parallel or antiparallel to electron velocity.[38] It is important to note that chiral structures favor the transfer of only one spin, but in principle, all excited electrons or holes can be transferred by chiral molecules. From a microscopic point of view, electrons are indistinguishable, and in a laboratory framework, each electron's spin has the same probability in all directions. Assuming sufficient time for electrons to pass through a chiral material, all excited electrons will be transferred through the chiral system with the 'correct' spin direction.

To explore the advantages of natural selection of chiral enantiomers in life processes, it is necessary to understand the mechanisms of the CISS effect. In general, spin polarized transport processes are associated with magnetic materials and large SOC. Hence most explanations for spin polarized transport in organic molecules are limited to introducing a large SOC in hydrocarbons, which is much larger than that observed experimentally.[39] Under the influence of SOC, electron spin is coupled with momentum, resulting in a certain correlation between the spin direction and velocity direction.[40] Chiral structures lead to an inhomogeneous charge distribution, resulting in a chirality-induced electric dipole moment inside the chiral molecule, which prevents the delocalization of electrons and makes them more localized.[41] Mirror symmetric chiral structures of enantiomers lead to mirror symmetric electron arrangement, which results in a mirror symmetric dipole electric field. $E_\perp$ is defined as the component of dipole electric field that is perpendicular to electron's velocity direction. When electrons move along the helical axis of chiral enantiomers, $E_\perp$ felt by electrons is in the opposite direction, which has opposite effects on the electron velocity. When considering the influence of chiral potential on electron spin, the SOC term in the Hamiltonian can be written as[42]

$$H_{\mathrm{SOC}} = -\frac{e\hbar}{2m^2c^2} s \cdot (p \times E_{\mathrm{chiral}}) = As \cdot l_{\mathrm{chiral}} \quad (2)$$

where E_{chiral} and l_{chiral} are potential and orbitals related to chirality. When the electron's velocity direction changes, the spin direction is also altered, resulting in an effective magnetic field that is generated by the joint action of the chiral structure

and electric dipole moments. This effective magnetic field controls electron's spin direction and breaks the degeneracy of spin energy levels in the chiral structure, which can be estimated using the motion law of charge in magnetic field. Suppose that an electron of mass m moves around in a chiral molecule with helix diameter d, then

$$\frac{d}{2} = \frac{mv}{e|B_{\text{eff}}|} \tag{3}$$

where e stands for electron charge and v stands for electron velocity. When d = 1 nm and the kinetic energy is 1 eV, SOC can be deduced to be about 390 meV, which is used to control electrons with one spin direction, while the SOC of C atoms is about 6 meV.[40] The presence of effective magnetic field has an amplifying effect on SOC in organic molecules. According to the relationship between magnetic field, Lorentz force and electron velocity, the direction of effective magnetic field should be consistent with the direction of electron transport, which explains why the spin direction tends to be parallel or anti-parallel to the velocity direction.[40] The theories reported earlier can be divided into three categories, the first of which is the tight binding model, used to describe the electron transfer through large helical molecules such as nucleic acids and oligopeptides.[43–47] The spin filtering efficiency strongly depends on the deoxyribonucleic acid (DNA) sequence, which is mainly determined from the combination of base pairs (bps).[44] The second is the spin dependent scattering theory.[48,49] The third is to consider large SOC from metal substrates[50] (such as Au and Ag) and induce spin selectivity during the transmission process through the selectivity of orbital angular momentum.[51] However, all these methods assume abnormally large SOC in chiral molecules and do not clarify how chiral structures and dipole moments affect spin polarized transport processes.[52]

In recent years, research on spin polarized transport of organic molecules has been increasingly improved, and new advances[53,54] have also been made in the theory of the CISS effect, which tries to explain from many perspectives and forms a diverse situation.

(i) Based on the Onsager reciprocal principle, Dalum *et al.*[55] proposed that the CISS effect disappeared when thermal averaging was performed on all electronic states, and attributed the generation of large SP to the existence of accidental degeneracy in molecular spectrum.

(ii) As a result of the interactions between molecules, charges on molecules are redistributed. Kumar *et al.*[56] proved that charge polarization in chiral molecules is accompanied by SP through measuring Hall signals, and speculated that SP imposes symmetry constraints on the biometric identification process, which ultimately leads to the selectivity between enantiomers.[57]

(iii) Most theories are based on the one-electron theory. Fransson[58] proposed the use of multi-body theory to account for the CISS effect, taking into account non-equilibrium conditions, electron correlation and electron–phonon coupling.[59] Compared to the uncorrelated model, SP of the model considering electron correlation is increased by 2 orders of magnitude. Recent studies[60] have demonstrated that the electron correlation caused by molecular vibration is crucial for the emergence of SP in systems composed of chiral molecules and ferromagnetic metals, where molecular vibration is a mechanism for breaking spin symmetry.

(iv) Lattice vibrations can induce additional electron tunneling processes, enhance electron coherence effects and improve SP.[61] Charge transport in chiral molecules is not isolated, but a product of the coupling of electrons with surrounding lattice distortion. Zhang *et al.*[61] proposed the polaron model to explain the CISS effect and showed that the coexistence of polaron and SOC leads to strong spin coherence and a high SP of up to 70%. In addition, it is found that the helical spacing should be much larger than the polaron size in order to obtain higher SP.[61]

(v) By calculating the relationship between SP and energy, it was found that the generalized Fano resonance features appear in the chiral polyacetylene system.[62] Based on the derivation and calculation of the Fano formula, it was found that a combination of two similar degenerate states produces a significant spin Fano resonance, the width of which increases linearly with the strength of coupling between the molecule and lead.[62]

(vi) On the basis of the electron correlation and vibration theory, Fransson and Naaman collectively came up with temperature-dependent experiments and theoretical models, emphasizing the importance of dissipation and the relationship between the CISS effect and optical activity.[63] The appearance of tunable high-order magnetic resonance in chiral spin soliton lattices suggests a link between vibration and spin.[64] Furthermore, dynamics suggests that CISS is a kind of phenomenon occurring in the excited state, implying that any mechanism that can maintain intrinsic spin anisotropy must account for excited state properties, such as electron–electron or electron–vibration interactions.[65] Subotnik *et al.* focused on how nuclear dynamics and Berry force manipulate electronic spin.[66,67] When the electronic current is non-zero, Berry curvature effects lead to spin separation of nuclear wave packets and SP of current, which could be considerable even with small SOC.

(vii) Based on the adiabatic perturbation method, effective Hamiltonian and unitary transformation, Geyer *et al.*[68] derived a simple analytical expression of the spin-dependent effective field and revealed its dependence on parameters. This theoretical model generates an effective SOC term independent of momentum, which demonstrates that SP is the result of broken time reversal invariance when selecting the given angular momentum of incident electron, which has no obvious dependence on the strength of SOC.[68]

(viii) The multi-orbital theory of the CISS effect states that electron correlation leads to strong instability of electron–hole pairs, which spontaneously breaks the spin and reflection symmetry.[69] Multi-body correlations caused by electron–hole pairs can produce a strong SOC at room temperature, which is sufficient to support the large SP observed in the CISS effect.

(ix) Some scholars believe that the free radical reaction in cryptochrome protein constitutes the basis for magnetic compass sensing in migratory birds.[70–72] In 2021, Luo *et al.* introduced the CISS effect in the electron transfer reactions of radical pairs and found that CISS enhanced the sensing to geomagnetic field in three ways.[73] Fay used the Nakajima–Zwanzig theory to explore the influence of electron transfer on the spins of chiral radical pairs, finding that chirality in intramolecular electron transfers generates specific coherent superpositions of spin states.[74] Moreover, in the discussion of Fay *et al.*, SP can be maximized for any non-zero SOC strength, which helps explain why large spin filtering phenomena occur in weak SOC systems.[24]

(x) Naaman *et al.*[75,76] further refined the dipole electric field hypothesis, explaining that the high spin selectivity of chiral molecules results from the interaction between helix-induced SOC and a strong dipole electric field, where it has also been confirmed that electron tunneling probability is strongly dependent on spin.

(xi) The interface theory[50,77] points out that, in addition to the chiral structure and large SOC in metal substrates, the origin of the CISS effect should also involve the spin transfer torque at spinterface composed of chiral molecules and metal electrodes, from which it can be concluded that greater interface distance will lead to lower spin transfer torque, which leads to the decline of SP.

In addition to the above explanations, some scholars have combined some theories or explored the source of large SOC in recent years. For example, Díaz *et al.*[78] proposed that the CISS effect originates from the dual contribution of dipole electric field and electron–lattice interaction. Based on the tight-binding model, Varela[79] and Torres[80] focused on hydrogen bonds in DNA and oligopeptides, respectively, showing that the spin activity of the CISS effect is determined from the intrinsic Rashba coupling of helices, and highlighting the great contribution of hydrogen bonds to SOC. Based on the interaction between electrode SOC, chirality and spin transfer torque at interfaces, Dobi[81] proposed the theoretical mechanism of the CISS effect in biomolecular junctions, opening a new way for the deeper understanding of chiral–spin coupling in biomolecules.

Despite the debate on the microscopic mechanisms, chiral molecules are widely regarded as spin filters,[82] through which one favored spin transmits and the opposite spin gets reflected. That is to say, the transmitted and reflected electrons exhibit opposite SP. Chiral molecule's preferred spin depends on the structural chirality. The spin filter hypothesis was further generalized to argue that a chiral molecule exhibits transient, opposite SP at two ends, which is usually used to rationalize experiments on the CISS effect.[83,84] For example, in 2014, three experimental measurements, including spin-polarized photoemission, cyclic voltammetry with magnetic electrodes and magnetic conducting probe atomic force microscopy (AFM) together demonstrated the spin filtering properties of helical peptides, as a function of length.[85]

However, it was demonstrated that SP is not necessarily conserved in electron transport processes. In 2017, Kumar *et al.*[56] used an innovative Hall device, without the presence of an external magnetic field, to show that a voltage-driven charge displacement in peptide molecules is accompanied by SP. Based on the orbital polarization effect, Liu *et al.*[86] pointed out that chiral molecules act as orbital polarizers and orbital filters in the processes related to the CISS effect, rather than spin filters. And in 2022, Wolf *et al.*[87] showed that the spin filter hypothesis contradicts the principle of prohibition of equilibrium spin current. Based on the unitary scattering matrix, it was proved that the transmitted and reflected electrons in the two-end CISS devices exhibit the same type of SP, which is actually universal in the two-end spintronic devices. More precisely, Wolf *et al.*[87] preferred to take chiral molecules as spin polarizers rather than spin filters. Chiral molecules polarize both transmitted and reflected electrons in the same direction, which depends on the structural chirality and electrons' incident direction. And the magnitude of SP depends on the local SOC in the CISS device. The spin polarizer theory provides a new way to understand CISS, which rationalized the anomalous Hall effect driven by the CISS effect.[88,89]

2.2. Theoretical calculations

Large atomic systems of helix structures and complex spatial structures of organic molecules bring trouble to the theoretical calculation, which leads to the slow development of the theoretical calculations related to the CISS effect. At present, most of the theoretical calculations reported are based on density functional theory (DFT) and first principles calculations, which are used to verify the mechanism or to complement experiments of the CISS effect. The calculation systems include glycine,[90,91] helicene,[92] carbon helix,[93,94] polyaniline,[95] methionine (MET)[96] and so on.

Based on theoretical calculations, Michaeli *et al.*[13] discovered that the electron transmission of chiral structures is larger than that of achiral structures. Fig. 2(a) displays the relationship between tunneling transmission, SOC strength and applied voltage. Fig. 2(b) shows the SP of chiral structures with different lengths under applied bias voltage, which predicts that SP is proportional to the molecular length. Volodymyr *et al.*[90] clearly demonstrated the influence of a helical structure on the spin polarized transport properties using a molecular junction model composed of Ni, Au and glycine, which complemented the experimental results[15,97] and promoted the understanding of the connection between helical structures and the CISS effect. In recent years, exchange interaction has gradually attracted the attention of scholars in the field of chirality.[91,95] Dianat *et al.*[91] used DFT to explore the influence of exchange interaction on the interaction between helical molecules and magnetic substrates, which showed the influence of exchange interaction on and the important role of helical molecules in magnetic response. From the photocurrent results of Fe_4N/MET/Fe_4N magnetic tunnel junctions based on the first principles quantum calculations,[96] it can be found that by adjusting the phonon energy and magnetization arrangement, *R*-MET

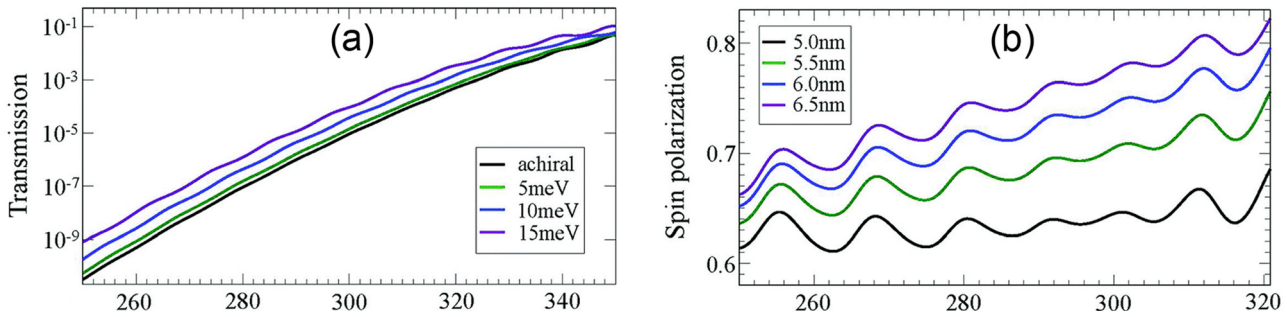

Fig. 2 Curves of (a) transmission and (b) SP as a function of applied voltage, where the color of the curves indicates the strength of SOC and the length of chiral molecules in (a) and (b), respectively. Reproduced with permission.[13] Copyright 2016©Royal Society of Chemistry.

molecules can output full spin polarized photocurrent with different spin channels. In addition, since the conventional SOC of atoms is not considered in the calculation method, this work is strong evidence for the source diversity of the CISS effect, that is, the spin–orbit correlation in chiral systems may not only be the contribution of conventional SOC inherent in atoms, but also include the contributions from electron correlation, SOC of electrodes, molecular chirality, spin transfer torque and so on.

Chiral molecules can effectively filter spin polarized electrons associated with metal contact and theoretical calculation has become an important way to study the correlation between chiral structures and electron spin. Based on the spin valve or tunnel junction model, the current value or transmission coefficient under bias voltage or light illumination is calculated through quantum transport calculations, which is a classical approach to estimate the CISS effect.

Recently, orbital texture has been shown to provide a topological perspective for understanding chirality in chemical and biological systems. Inspired by the chiral electronic structure of Weyl semimetals, Liu *et al.*[86] studied the orbital texture in the band structure, which is a topological feature caused by chirality. Orbital texture refers to the parallel or antiparallel relationship between orbital polarization L_z and momentum, which means that oppositely propagating electrons carry opposite orbital polarization. Because L_z is not a conserved quantity in molecules, it can be flipped during the transmission processes. Chiral molecules can polarize quantum orbitals in the charge transfer processes. Orbital polarization occurs when electrons are transferred from a chiral molecule to an inorganic lead, where orbital polarization causes SP due to SOC. Similarly, SP in the lead also causes orbital polarization due to the presence of SOC. Electron tunneling is affected by the matching relationship between the lead orbital polarization and the chiral molecule's orbital polarization, which results in chiral magnetoresistance. Conductance calculations confirm the orbital polarization effect in chiral helices, which is robust for temperature fluctuations and independent of the SOC from chiral molecules. Orbital texture provides a novel method to estimate the strength of the CISS effect in chiral materials.

2.3. Experimental techniques

Photoemission. Under light illumination, electrons that get enough light energy will be excited from the object surface and become photoelectrons, directional movement of which can generate a photocurrent. SP of the photoelectrons emitted from a gold substrate is 20% (−22%) under left-handed (right-handed) circularly polarized light, while zero under linearly polarized light.[10] When the gold substrate covered with a chiral film is irradiated with circularly polarized light, the intensity signal of the photoelectrons is monitored.[9] When the polarization of light changes from CW to CCW, the intensity signal changes significantly, indicating that the electron transport through chiral materials is spin dependent.[9] In addition, a Mott polarimeter was used to observe the CISS effect in 2011.[10] When electrons are scattered on the Au surface, the scattering angle depends on two factors, namely, the electron spin and incident angle. If the electron velocity direction (incident angle) was controlled by an applied electric field, the scattering angle distribution is only determined from the electron spin; this is why a Mott polarimeter can be used to detect the CISS effect. As shown in Fig. 3(a), linearly polarized light is used to illuminate the gold substrate.[10] Photoelectrons excited from the gold substrate will pass through the chiral structures and impinge on the polarization element, leading to a large angle scattering, which only depends on the electron spin. When the signal intensity of the two sides of the surface normal is different, it indicates that the chiral structure has spin filtering ability, which confirms the existence of the CISS effect.[10]

Electricity. Conductive probe AFM is a powerful tool for detecting the CISS effect. Fig. 3(b) shows the schematic diagram of experimental measurement, where the two ends of a chiral molecule are connected to Au and Ni.[98] Under an external magnetic field (permanent magnet), the magnetization arrangement of ferromagnetic Ni films can be reversed from 'up' to 'down'. Bias voltage is used to control the current direction, which ensures that spin polarized electrons generated by Ni films can pass through chiral molecules. The CISS effect can be verified from the current intensity in different magnetic field directions, where high current corresponds to the favorable spin of chirality and low intensity corresponds to the unfavorable one.

Electrochemistry. A redox probe is an important tool for detecting the CISS effect by electrochemical methods, where the efficiency of electrons passing through chiral structures is measured from the degree of redox reaction. As shown in Fig. 3(c), a permanent magnet is used to control the

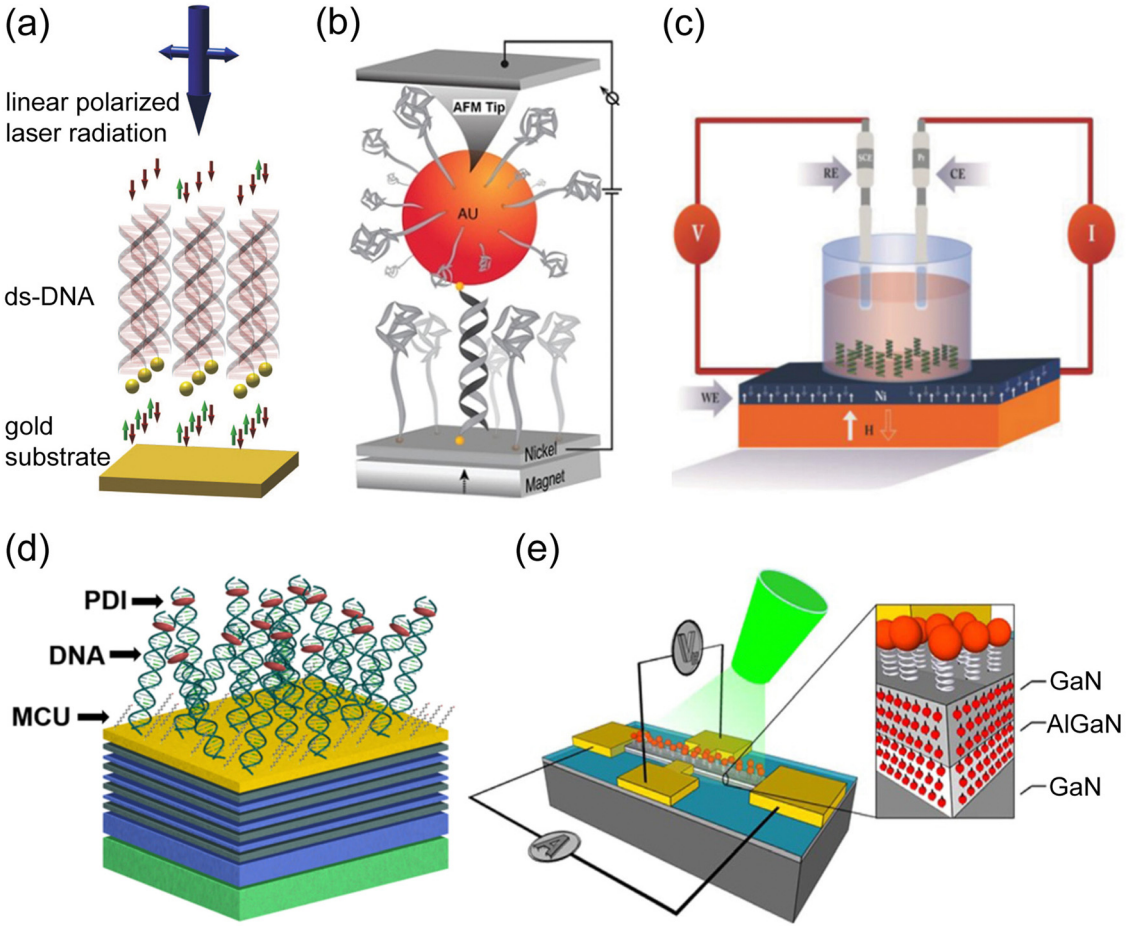

Fig. 3 (a) Experimental settings for verifying the spin filtering ability of ds-DNA by photoemission. Unpolarized photoelectrons are excited from the gold substrate by linearly polarized light. Reproduced with permission.[10] Copyright 2011©American Association for the Advancement of Science. (b) AFM experimental settings of the CISS effect. The Ni substrate is covered with monolayer DNA, which is absorbed by Au nanoparticles *via* mercaptan bonds. Reproduced with permission.[98] Copyright 2011©American Chemical Society. (c) Electrochemistry setup. The polymer is adsorbed on the Ni working electrode, which is magnetized by an external magnetic field with the magnetic dipole pointing up or down. Reproduced with permission.[99] Copyright 2015 © John Wiley and Sons. (d) Schematic diagram of a mixed monolayer of ds-DNA with associated fluorescent dye self-assembled on a gold-capped multilayer ferromagnetic substrate having perpendicular magnetic anisotropy. Reproduced with permission.[100] Copyright 2017©American Chemical Society. (e) Schematic structure of a GaN-based magnetless Hall device. Current flows between two electrodes and the Hall voltage is measured between the transverse set of electrodes. Nanoparticles are attached to the substrate through chiral molecules adsorbed on top of the conductive channel. Reproduced with permission.[101] Copyright 2016©Springer Nature.

magnetization direction of the Ni working electrode, which determines the spin direction injected into chiral structures.[99] By controlling the electric potential of metal substrates, a cyclic voltammetry curve is drawn to show the different transport barriers of opposite spin states, where a high barrier corresponds to the unfavorable spin and low barrier corresponds to the favorable one.

Fluorescence signals. An applied magnetic field is used to switch the spin direction of the ferromagnetic layer. Chiral mixed monolayers of double-stranded DNA (ds-DNA) with associated fluorescent dye self assembled on a gold-capped multilayer ferromagnetic substrate with perpendicular magnetic anisotropy. Close contact ensures the charge transfer between fluorescent dye molecules and ds-DNA. In order to exclude the influence caused by photo-induced charge separation and recombination in fluorescence molecules, the frequency and intensity of laser light were fixed. Under the experimental conditions used by Abendroth *et al.*, the degree of fluorescence quenching depends on the electron transfer efficiency from DNA molecules to metal substrates.[100] As the applied magnetic field direction changes, the fluorescence intensity shows significant differences, which can be attributed to the enhanced or suppressed effects of ds-DNA during the electron transfer process, as described using the CISS effect.

Hall probe device. When the applied magnetic field direction is perpendicular to the current direction, electrons and holes gather in opposite directions in a semiconductor due to the Lorentz force, resulting in a build-up potential. This phenomenon is called the Hall effect, and the build-up potential is called Hall voltage. A Hall device is a reliable method to detect the CISS effect. In GaN-based magnetless Hall devices, constant current flows between the two electrodes and Hall voltage is

measured between the transverse set of electrodes.[101] Experimental results showed that no Hall voltage was observed under dark conditions, while it was detected when the CdSe nanoparticles were illuminated with a laser. Further analysis according to the CISS effect shows that spin selective electron transport occurs when the CdSe nanoparticles are excited, which leads to spin dependent electron aggregation between CdSe and substrates, generating an effective magnetic field required by the Hall effect in the direction perpendicular to constant current. Thus, the magnitude of Hall voltage is proportional to the effective magnetic field caused by spin accumulation, whose symbol reflects the type of spin states (spin up or spin down).

In brief, there are many methods to measure spin selective electron transfer, the basic principle of which is eqn (1). Experiments aim to obtain signals that can reflect the number of spins passing through chiral materials, which can be reified as current, potential, magnetic field and even fluorescence intensity in different measurement methods. In addition to the several techniques detailed above, experiments using a magneto-optical Kerr device[102] and a capacitance device[103] have also been reported to explore the CISS effect.

3. Spin polarized electron transfer through chiral biomolecules

Organic molecules have attracted much attention in spintronics due to their long spin relaxation time and relaxation length. Dediu *et al.*[3] first reported that organic molecules can act as spin dependent transport channels and Xiong *et al.*[4] successfully designed the first organic spin valve. Light-induced charge transfer from achiral donor QDs depends on the spin and chirality of acceptor QDs.[104] Fe_3O_4 nanoparticles coated with chiral molecules effectively inhibited the formation of hydrogen peroxide as a by-product during the water decomposition experiment.[105] Furthermore, many biomolecules have chiral centers. The development of chiral drugs with high efficiency and low toxicity has become a hotspot in drug development and application.[106,107] Self assembled monolayers of polyalanine peptides were used to simulate biofilms to forecast the advantages of the CISS effect in life processes, where the combination of chirality and spin is anticipated to improve the accuracy of biometric identification.[13,108] In conclusion, the CISS effect has not only driven the revolution in spintronic devices, but also inspired a new round of exploration of life and Earth. Most biological macromolecules, such as nucleic acids, proteins and polysaccharides, exhibit chiral characteristics and tend to exhibit right-, left- and right-handed helices in the human body, respectively. Nature's preference to screen for one of the chiral enantiomers may imply a unique advantage of chiral–spin coupling in life.[13] Nevertheless, there are few reports analyzing and revealing the link between electron transport and life sciences from the perspective of biological system compatibility. This section summarizes the reports on charge transport of chiral biomolecules and discusses the advantages of chirality in the origin of organisms and life processes.

3.1. Nucleic acids and polysaccharides

Nucleic acids can be divided into DNA, ribonucleic acid (RNA) and peptide nucleic acid (PNA) in terms of composition, and divided into single-stranded (ss) and ds in terms of structure, where two ss-DNA with complementary bps can be hybridized to form self-assembled ds-DNA. In 2004, Nogues *et al.*[109] hybridized two ss-DNA with complementary bps to form self-assembled ds-DNA between Au substrates and Au nanoparticles. From reproducible conductivity measurements, it was found that at a bias voltage of ±2 V, ss-DNA exhibited insulating characteristics, whereas ds-DNA exhibited behaviors similar to those of a wide band-gap semiconductor with a current of 4 nA. This study demonstrates a significant difference in the conductivity of ss- and ds-DNA, meaning that ds-DNA is more likely to transmit charge. Ray *et al.*[110] and Guo *et al.*[111] proved from experimental and theoretical perspectives that ds-DNA has strong spin filtering activity, while ss-DNA almost has no spin polarized transport. Since then, the spin-selective transport of DNA has been mainly focused on ds-DNA.

Göhler *et al.*[10] used linearly or circularly polarized light with a photon energy of 5.84 eV to excite photoelectrons under ultra-high vacuum conditions, and used a Mott polarimeter to measure the SP of photoelectrons transmitted from the Au (111) substrate through self-assembled ds-DNA monolayers with different bp lengths (Fig. 4(a)). It was found that the self-assembled ds-DNA monolayer played a spin filtering role for the photoelectrons escaping from the Au (111) substrate, and the spin filtering ability increased with the increase in bp length. Monolayer ds-DNA consisting of 78 bps has a high SP up to 61%, proving the existence of spin polarized transport in chiral materials. Xie *et al.*[98] conducted research on spin selective electron conduction of ds-DNA molecules with ferromagnetic substrates, the experimental setup of which is shown in

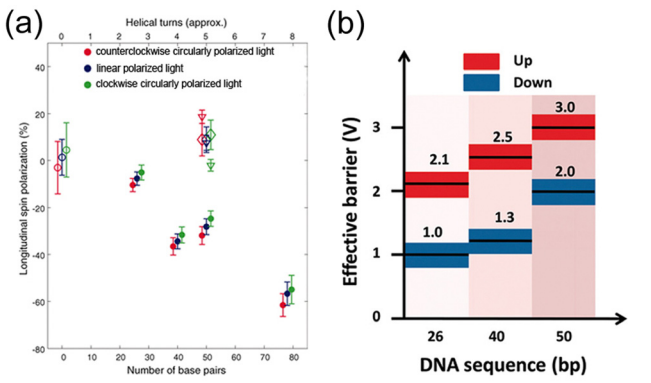

Fig. 4 (a) SP of electrons traversing monolayer DNA, including ds-DNA (filled circles), ss-DNA (open diamonds), damaged ds-DNA (open triangles) and polycrystalline Au (111) substrates (open circles). Reproduced with permission.[10] Copyright 2011©American Association for the Advancement of Science. (b) Effective barrier for the three oligomers with different bp lengths when the magnet is pointing up (red) or down (blue). Reproduced with permission.[98] Copyright 2011©American Chemical Society.

Fig. 3(b). The spin arrangement of Ni films was regulated by adjusting the placement of the permanent magnet, and the current carried by DNA was measured by AFM. The experiment showed that the effective barrier of ds-DNA would be adjusted according to the spin direction of electrons, as shown in Fig. 4(b), which explores the high spin selectivity of single ds-DNA at a molecular level and proves that the existence of spin polarized transport does not depend on chiral monolayers, making the construction of the theoretical model accurate for a single ds-DNA helix and reducing the difficulty of exploring spin polarized transport from a theoretical level.[98] Zhao *et al.*[112] proposed that the CISS effect of chiral organic molecules can be studied from three perspectives, chiral structure, SOC and spin dependent Anderson localization, and predicted the curve linear relationship between SP, bp length and energy by establishing a theoretical model of ds-DNA. Although many experiments have demonstrated that the spin polarized transport of DNA is related to chirality, the underlying mechanism is still unclear. In 2016, Zwang *et al.*[97] used electrochemical analysis to study the CISS effect of ds-DNA under fluid conditions. At high salt concentrations, CG-repeat sequences in the right-handed B-form can be flipped into a left-handed zigzag Z-form helix, both of which can be used as charge transfer media. It was found that the switch between two secondary structures (B- and D-) of ds-DNA can be used as the on–off switch of spin channels (Fig. 5(a)), indicating that the spin selective charge transport of ds-DNA depends on the secondary helical structure rather than the isolated molecular chiral center.

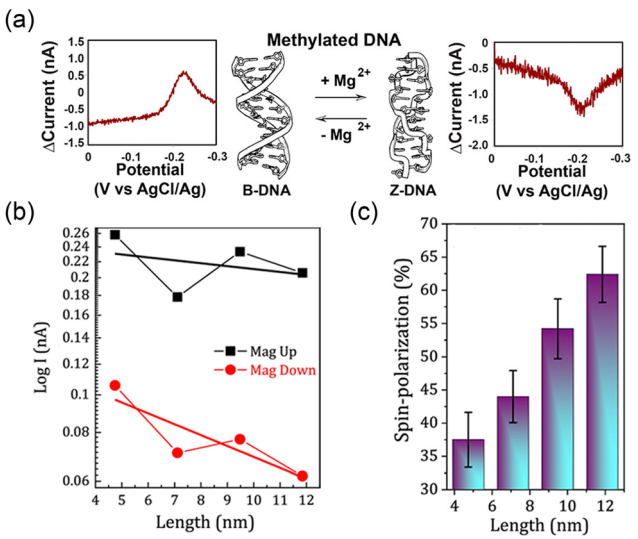

Fig. 5 (a) Representative data for 30 bp methylated $d(mCG)_{15}$. Data are plotted as the difference in current for a reductive sweep when the magnetic field is pointing up minus the current when the magnetic field is pointing down. Reproduced with permission.[97] Copyright 2016©American Chemical Society. (b) Length dependence of the current measured for ds-DNA at a bias voltage of 1 V. Slopes of the linear fits are in a ratio of 3 : 1. (c) Histogram summary of SP for various lengths of ds-DNA at a bias voltage of 2 V. Reproduced with permission.[115] Copyright 2020©American Chemical Society.

Early research methods on the charge transport of chiral organic molecules are mainly divided into four types, which are photochemical technology for solution environments, electrochemical methods for DNA attached to surfaces, organic molecules as connecting medium and a photoemission method.[113] In 2017, Abendroth *et al.*[100] creatively used fluorescence microscopy to observe spin-dependent charge transport in self-assembled ds-DNA monolayers on ferromagnetic substrates, expanding the observation way of the CISS effect. In recent years, the focus of research on spin selective charge transport of DNA molecules has gradually shifted to the mechanism of CISS. In 2015, Naaman and Waldeck proposed that CISS is a result of the combined effect of SOC and chiral molecular dipole electric field.[40] Salazar *et al.*[114] believed that intermolecular tension was the breakthrough to explain electron mobility and spin selective transport in DNA molecules, and took SOC as a function of the DNA structure and deduced the variation in molecular kinetic energy and SOC in ds-DNA under longitudinal compression or tensile strain through the Slater–Koster model. The results indicate that longitudinal stretching can enhance SOC and compression can weaken SOC, which is of great significance for the investigation of the CISS effect in DNA molecules, demonstrating that SP of electron transport through chiral molecules may be regulated by applying strain. In 2020, Mishra *et al.*[115] measured the charge transfer and SP induced by electric field of ds-DNA with different lengths, which are shown in Fig. 5(b) and (c). In the length range studied (4–12 nm), the SP of carriers is almost linearly related to the DNA length, but the spin conduction of DNA molecules is a nonlinear process. In addition, by fitting the length of ds-DNA and current, it can be seen that the linear fitting slope ratio is 3 : 1 when the magnet direction is opposite, namely, the unfavorable spin decays three times faster than the favorable one, which shows that due to the coupling of linear momentum and spin, the transmission of favorable spin is almost unaffected by backscattering. In addition, new progress has also been made in the mechanism research from a theoretical perspective. Du *et al.*[116] found the enhanced effect of electron–vibration interaction on CISS by introducing the Lang and Firsov transformation based on the Hamiltonian of ds-DNA, providing a feasible way to detect vibration-induced SP in low-dimensional helices.

The DNA analogue, PNA, can be obtained by replacing the sugar phosphate backbone with an amino acid backbone, which can recognize and bind DNA or RNA sequences through complementary bps to form stable double helix structures. Mollers *et al.*[117] researched the CISS effect of self-assembled ds-PNA monolayers, finding that under polarized light illumination, PNA containing chiral centers exhibited spin filtering characteristics with an SP of 24%, while the helical PNA with no chiral centers had a small SP value of 12%, as shown in Fig. 6. The results confirmed that the preferred carrier spin orientation was directly related to the helix handedness, and indicated that the introduction of chiral centers could enhance the spin filtering ability of double helices, which was consistent with the discovery of spin selective transport in ds-DNA.[97]

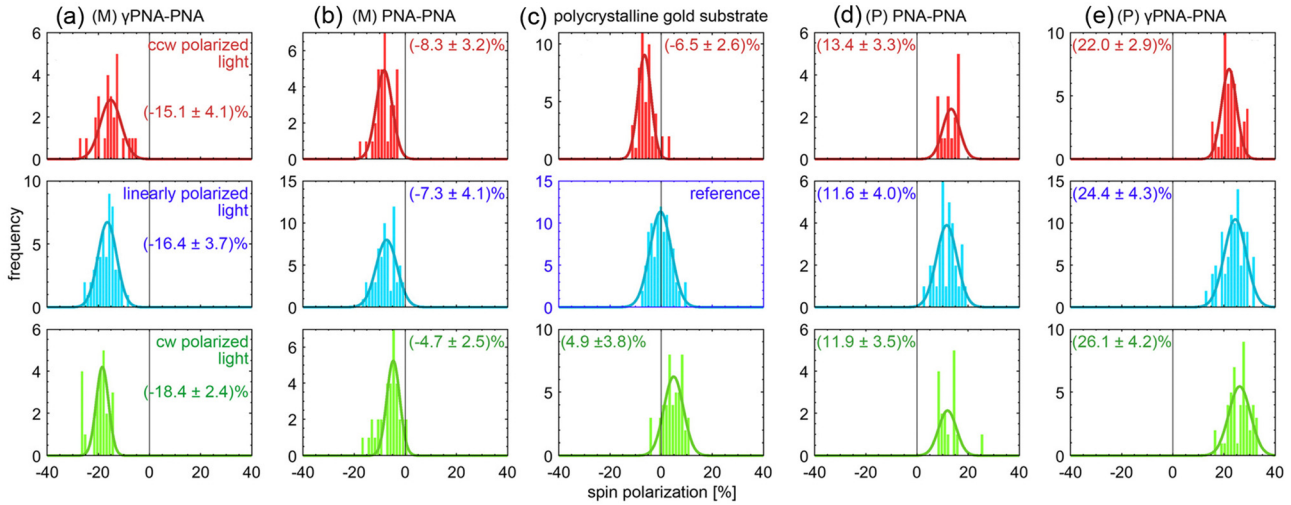

Fig. 6 SP of photoelectrons transmitting through the left (M) and right (P) helices of (b), (d) PNA–PNA consisting of achiral monomers and (a), (e) γPNA–PNA containing numerous chiral monomers. (c) Measurements on bare gold. Red, green, and blue represent measurements under excitation of CCW circularly polarized, CW circularly polarized and linearly polarized light. Reprinted with permission.[117] Copyright 2021©John Wiley and Sons.

Single wall carbon nanotubes (SWCNTs) are a spin filtration material wrapped with a ss-DNA helix, as shown in Fig. 7(a). In 2015, Alam *et al.*[11] experimentally reported the spin polarized transport in SWCNTs wound by ss-DNA consisting of 30 alternating G and T bases ($d(GT)_{15}$) for the first time. Ss-DNA provides a chiral potential field and SWCNTs provide a charge channel. A combination of these two overcomes the obstacles in the study of the spin selective transport in ss-DNA due to poor conductivity. According to the magnetoresistance measurement, it was found that the hybrid system can be used as a spin filter. The SP decays with an increase in temperature or bias, which reaches saturation at 0.35 V and is close to 74% at a low temperature of 12 K, as shown in Fig. 7(b) and (c).[11] In order to study the universality of the CISS effect in ss-DNA wrapped SWCNTs, Alam *et al.*[118] used $d(T)_{30}$ as ss-DNA to conduct experiments on the CISS effect by hybridizing SWCNTs, where the magnetoresistance measurement indicates that SP reaches 80% and retains the characteristics that decay with the increasing temperature or bias. These two works demonstrated the existence of spin selectivity in ss-DNA and restarted the research on spin polarized transport of ss-DNA by hybridizing with SWCNTs. Chiral potential induces a coupling between carrier momentum and spin, based on which Rahman *et al.*[119] proposed the idea of regulating carrier spin through the interaction between DNA and SWCNTs, and constructed a spin filter composed of SWCNTs and ss-DNA, where the SWCNTs were modified with ss-DNA sequences consisting of $d(AC)_{15}$ and $d(CC)_{15}$, respectively. The results show that different DNA sequences induce different degrees of SP, indicating that SP of carriers in nanotubes can be adjusted by constructing specific DNA sequences, which provides a feasible scheme for the application of CISS effect, that is, SP of conductive materials can be induced by the helical functionalization of specific bps. In addition, magnetoresistance effects also appeared in the hybrid system made up of SWCNTs and ss-DNA. Rahman *et al.*[120] used SWCNTs wrapped with $d(AC)_{15}$ to explore the connection between magnetoresistance and the CISS effect, and speculated that in a low temperature range, SP induced by the CISS effect could increase the carrier localization length by an order of magnitude, and then affect the magnetoresistance.

Earlier studies on self-hybridizing ss-DNA have demonstrated the stability of hairpin DNA at room temperature, which can be used as molecular beacons to identify DNA molecules at the base level.[121–123] However, the spin polarized charge transport in hairpin DNA is still unclear. The CISS effect enables the chiral helix to have spin filtering ability, which is enhanced with the increasing number of spirals.[124] Stemer *et al.*[12] found spin dependent and chiral selective electron scattering through the photoemission process of chiral self-hybridizing ss-DNA monofilms, where Hg^{2+} binds specifically to the base *T*, enabling exact control of the amount and location of Hg^{2+} on hairpin DNA helices. The spin selective charge emission of ferromagnetic substrates modified with mercurized DNA helices was measured under ultraviolet (UV) light. For the case of hairpin DNA monolayers containing Hg^{2+}, charges with different spin directions exhibited photoionization energy dependent on the substrate magnetization, and for the case without Hg^{2+}, charge emission in different spin directions showed no difference (Fig. 7(f)–(i)). In addition, when the increasing amount of Hg^{2+} induces an inversion of the secondary structure of DNA helices, the spin selectivity will also reverse.[12]

From the point of view of the primary structure, chiral centers of both polysaccharides and DNA are located in the monosaccharide components (usually glucose and deoxyribose). Cellulose nanocrystals (CNCs) are composed of chiral cellulose units that can self-assemble to form left-handed helical laminas under dry conditions, where the arrangement of the secondary structure varies with the applied magnetic or

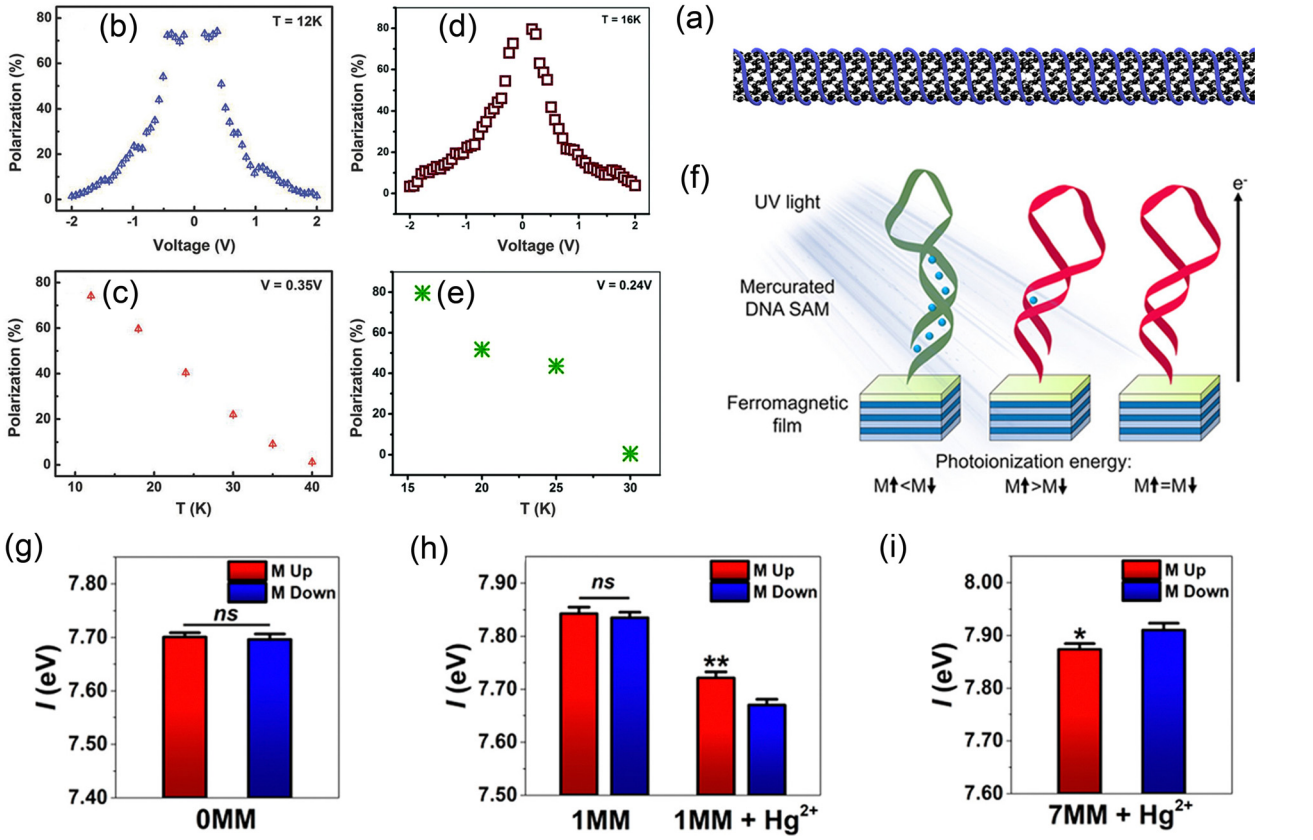

Fig. 7 (a) Schematic diagram of the composite structure of ss-DNA wrapped SWCNTs. Reproduced with permission.[119] Copyright 2020©American Chemical Society. The polarization is considered as a function of the voltage (V) and temperature (T). The polarization of SWCNTs coated with $d(GT)_{15}$ as a function of (b) V and (c) T. Reproduced with permission.[11] Copyright 2015©John Wiley and Sons. The polarization of SWCNTs coated with $d(T)_{30}$ as a function of (d) V and (e) T. Reproduced with permission.[118] Copyright 2017©Royal Society of Chemistry. (f) Schematic diagram of the structure of self-hybridizing ss-DNA (DNA hairpins), where the increasing Hg^{2+} results in a change in the chirality of hairpin DNA from right-handed helix (red) to left-handed helix (green). Photoionization energies collected under field up (red) and down (blue) substrate saturation magnetization conditions for self assembled monolayers of (g) 0MM, (h) 1MM and 1MM + Hg^{2+} and (i) 7MM + Hg^{2+}; error bars represent the standard errors of the mean. Reproduced with permission.[12] Copyright 2020©American Chemical Society.

electric field (Fig. 8(a)). Hammam *et al.*[125] believed that the driving force for the changing secondary structure comes from the electron spin, which emphasizes the importance of the CISS effect in polysaccharides. The measurement results of Hall resistance showed that 1,2,3,4-butanetetracarboxylic acid enhanced the packing density of the helical structure of CNCs (Fig. 8(d)), resulting in an increase in Hall resistance. In addition, Hall resistances measured under different magnetic field orientation conditions are different, which proves the CISS effect of CNCs, as shown in Fig. 8(g) and (h).

3.2. Amino acids, oligopeptides and proteins

Gene expression is achieved through the synthesis of proteins controlled by DNA, which are involved in almost all life processes and considered to be the direct executor of life activities. Studying the effect of spin on charge transport in proteins or amino acids is the key to understanding charge transport in life activities. The CISS effect was proposed based on the transmission measurement of polarized and unpolarized photoelectrons passing through 5 layers of L- or D-stearoyl lysine films,[9] which stimulated the research studies on the relationship between chirality and spin. Carmeli *et al.*[108] used the self-assembled monolayers of α L- or D-polyalanine polypeptides to simulate biofilms and found that adsorption converted electric dipoles into magnetic dipoles, which made the polyalanine polypeptide films magnetic.

Mishra *et al.*[126] conducted spin dependent photoelectron transport and electrochemical studies on purple films containing bR deposited on different substrates. The results (Fig. 9) showed that purple films containing bR show spin selective charge transport, where the SP is about 15%. In addition, the CISS effect is a characteristic of a chiral system and independent of the substrate, which may occur in biological systems and play an important role in the high efficiency electron transfer process of helical proteins. Photosystem I (PSI) exists in plants and is one of the electron transfer systems for photosynthesis. SP of electron transfer can be assessed by controlling the orientation of PSI monolayers relative to the Ag substrate. Experimental results show the spin selectivity of PSI throughout the whole charge transfer path, which reaches

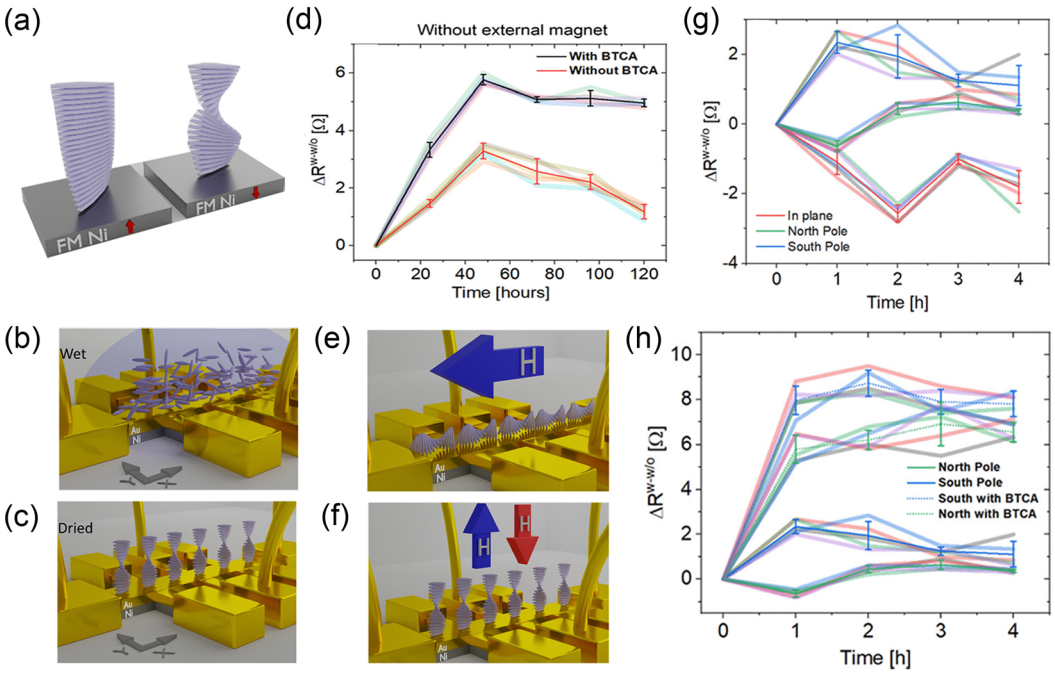

Fig. 8 (a) Changes in the secondary structure of cellulose CNCs in an applied magnetic field. (b) and (c) Configuration scheme of the anomalous Hall effect sensor. In (b), the cellulose CNCs are in the wet phase, so they are not arranged into chiral structures and have low resistance. In (c), cellulose CNCs arrange into chiral structures when dried. (d) Hall resistance of cellulose CNCs. In the absence of an external magnetic field, the Hall resistance reaches its maximum value around 48 h. (e), (f) Anomalous Hall effect sensor configuration schemes and (g), (h) Hall resistance measurement results of cellulose CNC samples under vertical and in-plane magnetic fields. Reproduced with permission.[125] Copyright 2022©American Chemical Society.

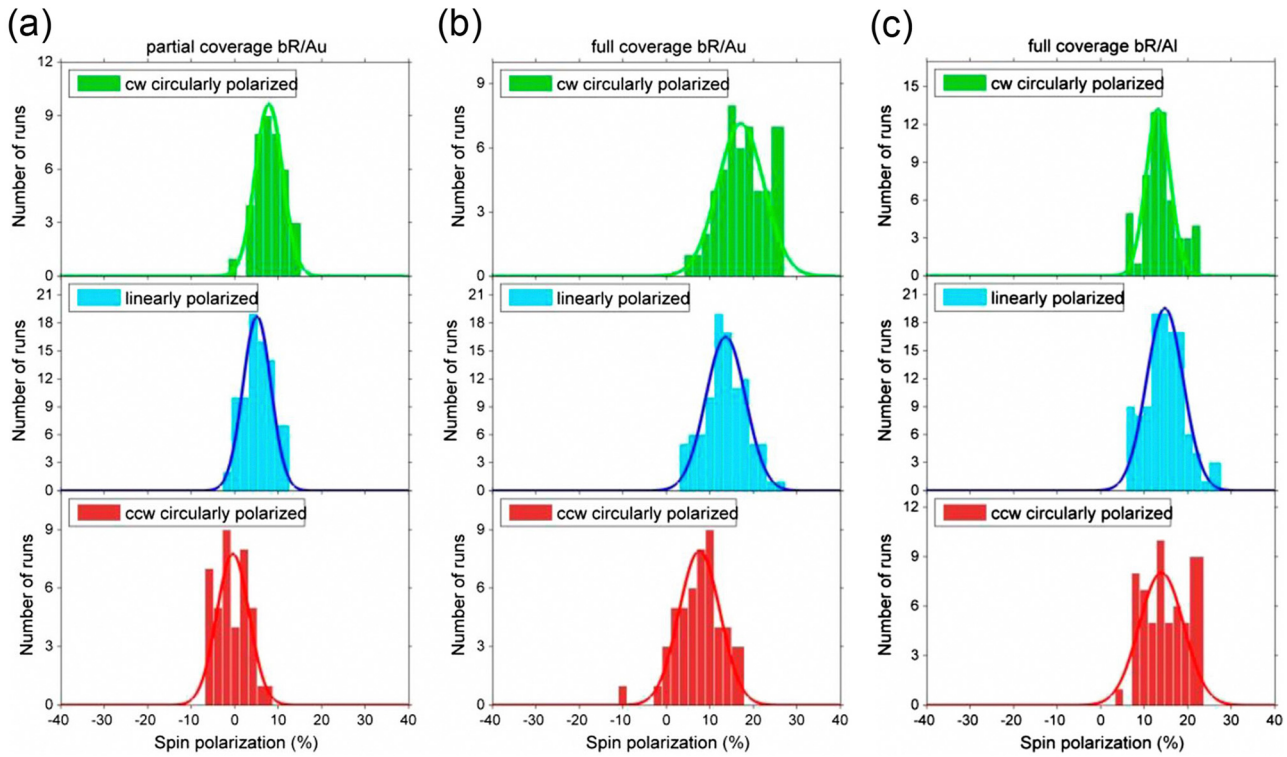

Fig. 9 SP of photoelectrons after having traversed a purple membrane containing bacterial rhodopsin 10% in volume adsorbed on (a), (b) gold and (c) Al substrates. Red, green and blue represent the measurement results under excitation of CCW circularly polarized light, CW circularly polarized light and linearly polarized light. Reproduced with permission.[126] Copyright 2013©National Academy of Sciences.

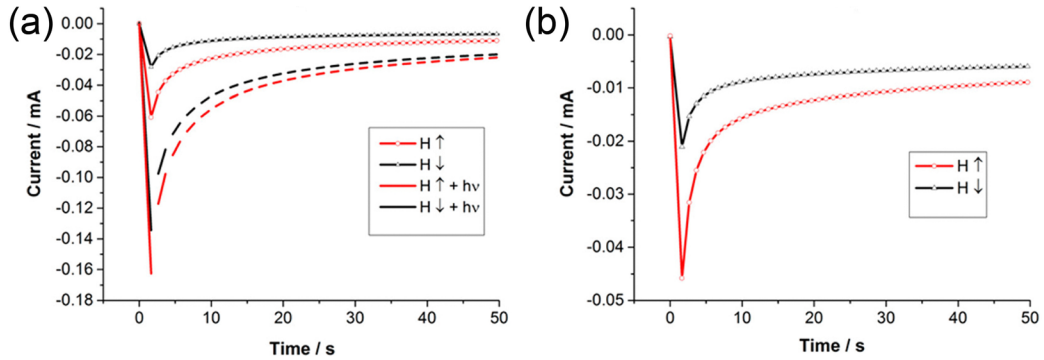

Fig. 10 Chronoamperometric measurements of (a) mutant D96N bR and (b) wild-type bR on Ni substrates, with the magnetic field pointing up (red line) or down (black line) under laser illumination at a wavelength of 532 nm. Reproduced with permission.[27] Copyright 2015©American Chemical Society.

the peak value at 300 K and disappears below 150 K.[127] Carmeli *et al.*[127] proposed the conjecture that the chiral structure of protein complexes plays an important role in determining high spin selectivity and temperature dependence. These two experiments demonstrated the existence of the CISS effect in animal systems and botanical systems, verifying the possibility of spin directed electron transfer in organisms. Since then, most experiments have focused on the factors influencing CISS, including light,[27,96] environmental humidity,[85] structure,[15,84,90,115] bias[128] and temperature.[101,129]

Einati *et al.*[27] studied the light-operated spin filtering of bR and its D96N mutant, as shown in Fig. 10(a) and (b), which shows that the spin filtering ability of the D96N mutant was significantly reduced under light illumination, while that of wild-type bR was not affected. This experiment proves that light can regulate the degree of SP and provides a basis for studying the relationship between the protein structure and spin filtering ability. Based on the magnetic tunneling junction model, Xu *et al.*[96] explored the regulation of spin dependent transport characteristics of chiral MET molecules by light and magnetic field. MET molecules can output fully spin polarized photocurrent with different spin channels by adjusting the photon energy and magnetization arrangements, which can be used as switches of the spin channel and photocurrent direction. When the phonon energy is 4.5 eV, *R*- and *S*-MET molecules tend to transport electrons with different spin directions, demonstrating the existence of the CISS effect.[96] This work provides a theoretical basis for understanding the magneto-optical coupling of chiral molecules and life sciences, showing that the spin transport process of amino acids can be modulated by multiple fields, accompanied by a variety of switching effects that control spin channels and the photocurrent direction. Kettner *et al.*[85] proposed a measurement method for charge transport in oligopeptides at room temperature and established the dependence of electron transfer and spin filtering ability on the secondary helical structure, which shows that the CISS effect is environmentally stable and insensitive to the spatial environment (dry or wet). As shown in Fig. 11(a) and (b), the CISS effect disappears when oligopeptides are denaturated. In the length range studied (2–3 nm), SP of charge transport is

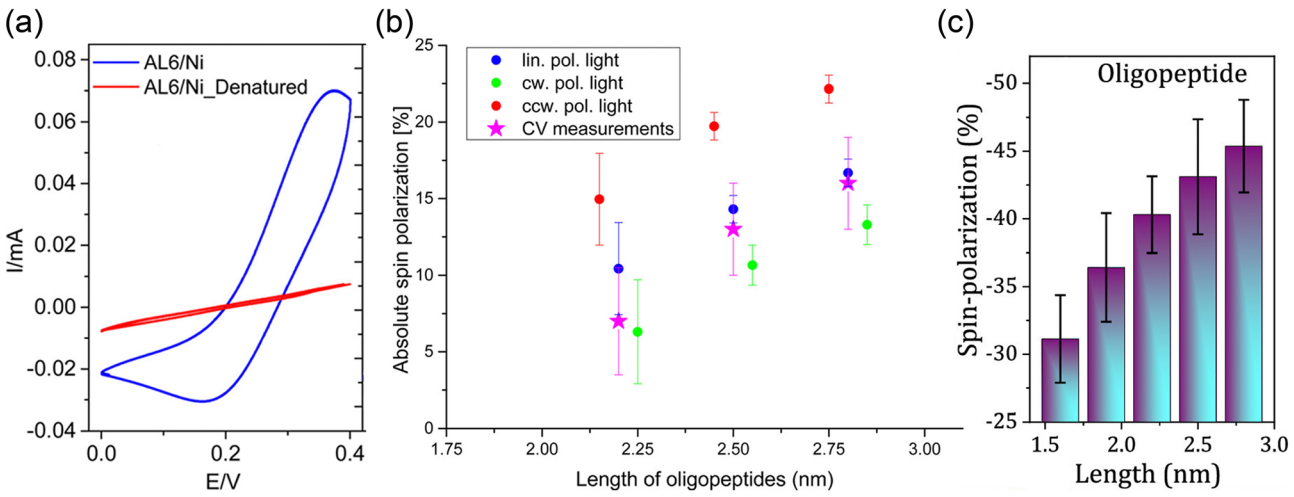

Fig. 11 (a) Voltammograms of Ni electrodes coated with self assembled oligopeptide monolayers measured before (blue) and after (red) denaturation. (b) Dependence of the absolute value of longitudinal SP on oligopeptide length. Reproduced with permission.[85] Copyright 2015©American Chemical Society. (c) Histogram summary of SP for various lengths of oligopeptides at a bias voltage of 2 V. Reproduced with permission.[115] Copyright 2020©American Chemical Society.

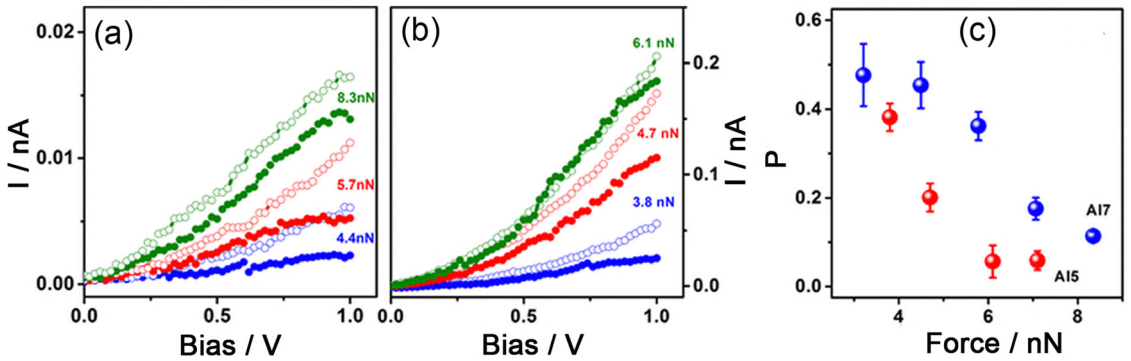

Fig. 12 Average *I*–*V* data for (a) Al7 and (b) Al5 oligopeptide monolayers recorded under various tip loading forces when the tip was magnetized by positive (solid circle) or negative (hollow circle) magnetic fields. (c) SP of Al5 (red) and Al7 (blue) oligopeptide monolayers as a function of tip loading force at a bias voltage of 1 V. Reproduced with permission.[84] Copyright 2017©AIP Publishing.

proportional to the length of oligopeptides, and the spin filtering efficiency per unit length of oligopeptides is more than twice that of DNA, meaning that the thickness of the spin filter composed of oligopeptides is smaller.[15] The dependence of charge transport on oligopeptides' structures was investigated through magnetic conductive probe AFM.[84] Experimental results show that the spin selectivity increases with the increase in chiral length, which is consistent with the report that SP was proportional to the length of oligopeptides, as shown in Fig. 11(c).[115] Spin filtering ability of oligopeptides can be regulated by strain. When the tip loading force increases, the chiral molecules tilt and the tunneling distance is shortened, which leads to an increase in the current in chiral layers.[84] The spin selectivity of oligopeptides decreased with the increase in tip loading force, which is attributed to the increasing ratio of spiral radius to pitch and the increasing tilt angle between the molecular axis and surface normal (Fig. 12(c)). In addition, research studies on the relationship between the CISS effect and helical structure have also been reported based on DFT, which indicate that magnetoresistance of α-helix glycine oligopeptides in molecular junctions is about 100–1000 times that of β-chains, suggesting that the helical structure plays a key role in enhancing SP associated with the CISS effect.[90] The effect of bias voltage on spin polarized electron transport was speculated based on the effective model Hamiltonian and Landauer–Büttiker formula.[128] By calculating the conductance and SP of α-helix peptides in contact with non-magnetic electrodes, it has been found that the spin filtering efficiency can be improved by appropriately adjusting the magnitude and direction of bias voltage. When the bias voltage is 0, SP will increase monotonically with the length of α-helix peptides, otherwise SP will oscillate. It was found that the structure of oligopeptides is highly dependent on temperature.[101] Similar to the low-temperature denaturation process of polypeptides, the α-helix structure based on alanine and aminoisobutyric acid changes to a linear structure at low temperature, which initiates a rearrangement of hydrogen bonds and a reversal of electric dipole moment orientation accompanied by a change of the spin channel, opening a new possibility to control electron spins in organic spintronic devices.[101]

Similar to the idea of ss-DNA hybrid SWCNTs, hybrid chiral–achiral materials have also been reported in the field of amino acid molecules. Michaeli *et al.*[13] applied optics and spintronics to a hybrid system composed of organic molecules and semiconductor nanoparticles, and compared the photoinduced charge transfer process of chiral polyalanine and achiral hexadecane dithiol adsorbed on the Au substrate. The experimental setup is shown in Fig. 13(a), where the self-assembled organic monolayer is adsorbed on the Au electrode, and CdSe nanoparticles are attached to the top of organic monolayer. A Kelvin probe is used to measure the work function variation of organic molecules, results of which show that ΔCPD of chiral polyalanine is an order of magnitude larger than that of achiral hexadecane dithiol. ΔCPD is positive in the case of chiral polyalanine, indicating that hole transfer is more efficient than electron transfer during the transport *via* polyalanine. Mondal *et al.*[26] followed the idea of a hybrid system of organic molecules and CdSe nanoparticles, and replaced the Au substrate with Co and explored the spin dependent photoinduced charge transfer process of hybrid oligopeptide-CdSe deposited on a ferromagnetic substrate by electrochemical and photoluminescence methods. Under the illumination with a green laser at a wavelength of 514 nm, the current passing through chiral layers changes with the magnetic orientation, where the illumination results in the reversal of the SP and decrease in the absolute value, as shown in Fig. 13(c)–(e). The experiments show that the photoluminescence intensity of nanoparticles can be controlled by adjusting the magnetization direction of the substrate and the photosource can be used as a switch for the spin channel. In electrochemical cells, the combination of CISS and durable luminescent materials shows unique advantages in the sensing of arginine enantiomers, and opens up a new way for enantiomer selective sensing. Zhang *et al.*[130] designed a ternary structure composed of inorganic durable luminescent Pr^{3+}:$CaTiO_3$ with Ag nanoparticles coated with cysteine molecules, as shown in Fig. 13(f), where the electrons in Pr^{3+}:$CaTiO_3$ will be transferred to Ag nanoparticles through the heterostructure, and then captured by cysteine molecules. UV illumination promoted the electron transport in this study and fast selective sensing of enantiomers was achieved based on the CISS

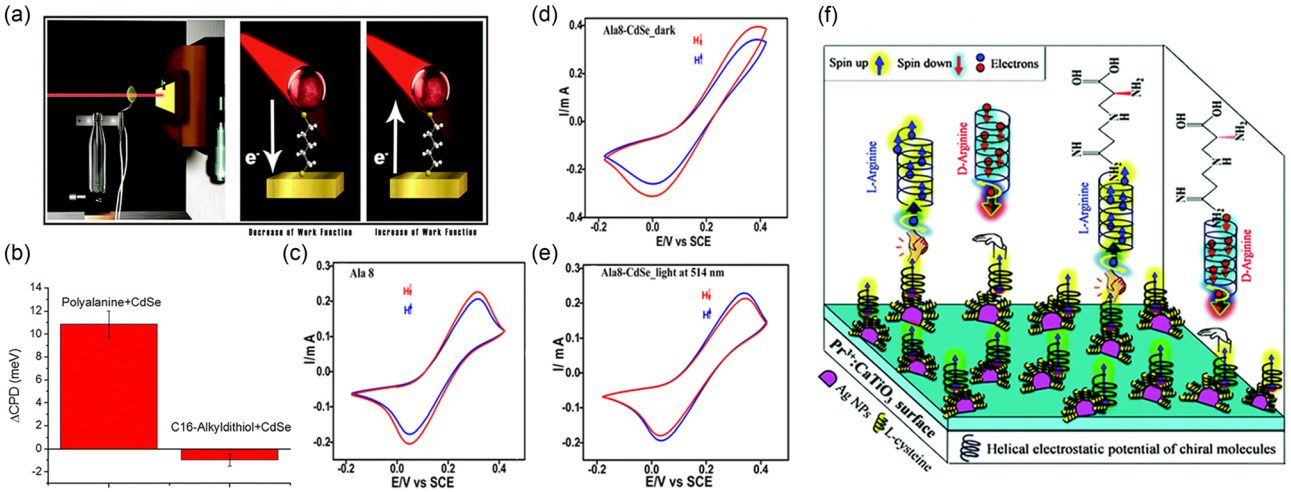

Fig. 13 (a) Kelvin probe setup for measuring surface work function variation under illumination. When electrons are transferred from CdSe nanoparticles to the substrate under light excited (middle figure), the measured work function decreases, otherwise (right figure), the work function increases. (b) Changes in the work function of chiral polyalanine and achiral hexadecane dithiol. Reproduced with permission.[13] Copyright 2016©Royal Society of Chemistry. Spin dependent cyclic voltammograms of (c) Ala8 monolayers adsorbed on ferromagnetic substrates and Ala8-CdSe hybrid structures under (d) dark and (e) light conditions. Reproduced with permission.[26] Copyright 2016©American Chemical Society. (f) Enantiospecific interaction between the Pr^{3+}:$CaTiO_3$@Ag@L-cysteine surface and chiral arginine due to the CISS effect. Reproduced with permission.[130] Copyright 2019©Royal Society of Chemistry.

effect.[130] Besides binding to nanoparticles, chiral amino acids can also be hybridized with molecular wires to investigate the conduction of spin polarized currents in achiral structures. Measurements of spin polarized current generated by tunneling of right-handed helical proline oligopeptides based on conducting atomic force microscopy with magnetic tips and spin Hall devices indicate that spin polarized currents can be well maintained in achiral molecular wires, where the current density can be modulated by changing the length of conjugated components.[131] As shown in Fig. 14(d)–(f), on increasing the length of PZn_n molecular wire, spin selectivity of Pro_8PZn_n and difference in the effective barrier for opposite spin states both increase, indicating that chiral structures are not necessary for spin current conduction and polarized current generated by the CISS effect can further propagate in achiral structures.

Aragonès *et al.*[14] measured the spin filtering ability of single chiral peptides for the first time, making spin dependent electron transport accurate at a molecular level. The direction of electron transport was controlled by the applied bias voltage, which ensures that electrons are transferred from the Ni tip to the Au electrode, as shown in Fig. 15(a). Conductance is proportional to the electron transmission and higher

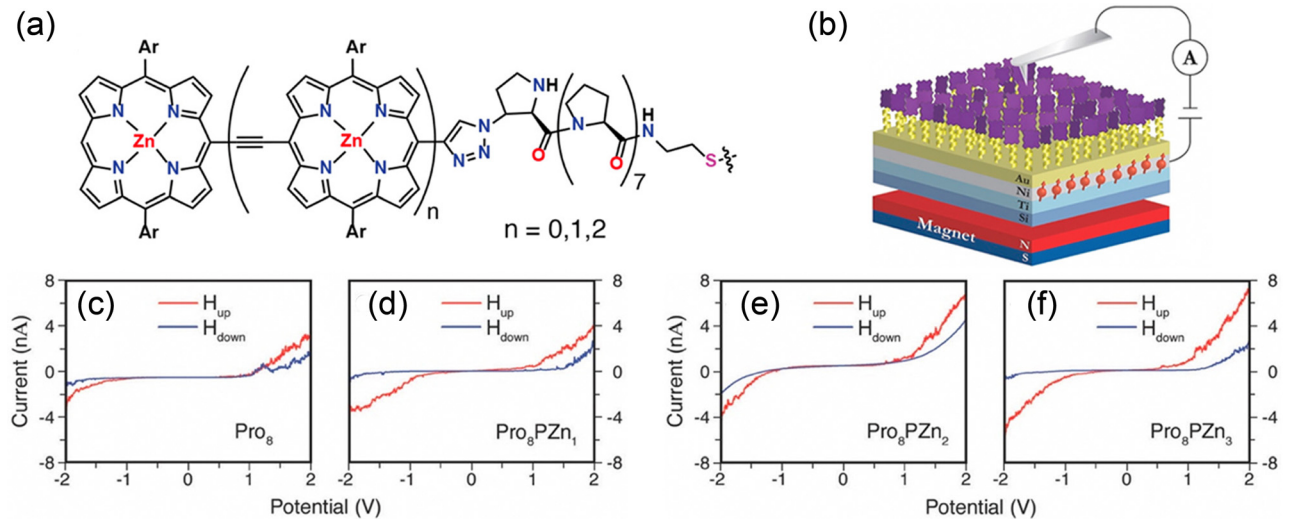

Fig. 14 (a) Structures of Pro_8PZn_n molecules. (b) Schematic diagram of the experimental setup for magnetic conductive AFM measurements. *I*–*V* responses of (c) Pro_8, (d) Pro_8PZn_1, (e) Pro_8PZn_2 and (f) Pro_8PZn_3, where blue and red represent different magnetic field orientations. Reproduced with permission.[131] Copyright 2019©American Chemical Society.

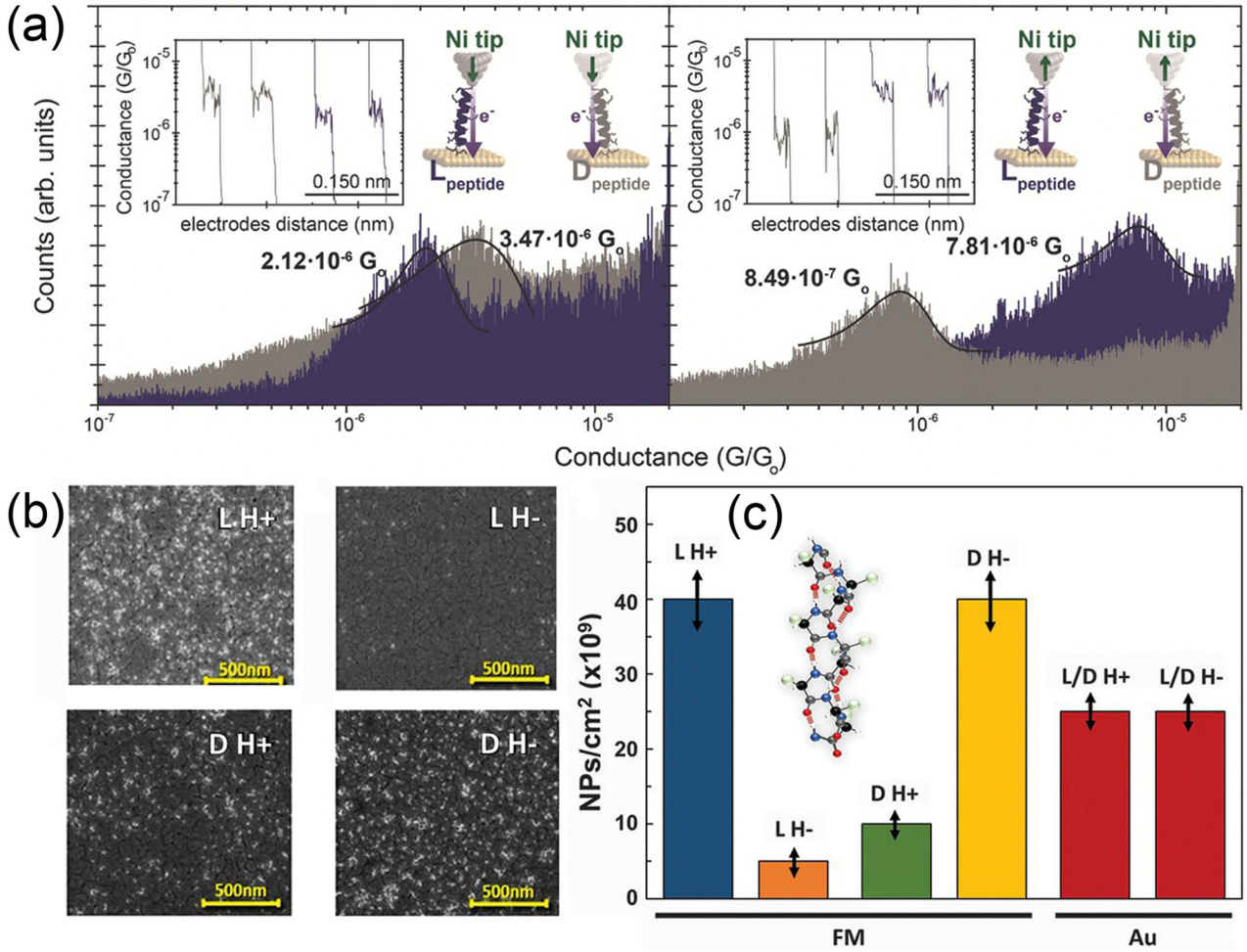

Fig. 15 (a) Semilog conductance histograms of right-handed and left-handed peptides when the magnetic polarization of the Ni tip is up and down, where the insets show representative current *versus* pulling traces used to construct the conductance histograms. Reproduced with permission.[14] Copyright 2016©John Wiley and Sons. (b) Adsorption of polyalanine oligopeptides on ferromagnetic substrates, where the magnetic dipole points up (H+) or down (H−) relative to the substrate surface. SiO_2 nanoparticles were attached to the adsorbed oligopeptides. (c) Adsorption density of SiO_2 nanoparticles under different conditions, and the double arrows represent error bars. Reproduced with permission.[132] Copyright 2018©American Association for the Advancement of Science.

conductance corresponds to the preferred spin direction of chiral peptides. When the magnetic polarization of the Ni tip is down, the conductance of the D-peptide is larger, while when the magnetic polarization is up, the conductance of L-peptide is larger, indicating that magnetic orientation affects the charge transport process of peptide molecules, two enantiomers of which have opposite spin preference. Similarly, most studies[12,25,26,98,100] on the systems made up of chiral molecules and ferromagnetic substrates have confirmed that the magnetic direction of substrates affects the spin polarized transport through chiral molecules. But the interaction between chiral molecules and ferromagnetic substrates is not definite, which may have important applications in enantiomer recognition and separation. Banerjee-Ghosh *et al.*[132] proved experimentally the interaction between chirality and vertical magnetized substrates which is not controlled by magnetic field, but by the electron spin direction. The number of SiO_2 nanoparticles attached to chiral polyalanine oligomers is taken as a marker of the adsorption density per monolayer, as shown in Fig. 15(b) and (c). According to scanning electron microscopy, the particle concentrations of L- and D-polyalanine on magnetic substrates with different magnetic directions are complementary, while those of L- and D-polyalanine on non-magnetic substrates exhibit no enantioselectivity. Ghosh *et al.*[133] further studied the enantioselective interactions between ferromagnetic substrates and chiral molecules using Kelvin probes, and found that electron transport from an electrode to chiral molecules depends on the magnetic direction of the ferromagnet and molecular chirality through the spin related contact potential difference. Enantioselective interaction between a ferromagnetic substrate and chirality depends on the magnetization intensity, magnetization direction, molecular chirality and thickness of the substrate.

In recent years, the research direction on the CISS effect of amino acids has gradually shifted from exploring the basic transport properties to using the spin filtering ability to

manufacture spintronic devices,[18,19,134,135] improving the efficiency of electrochemical reactions[136,137] and promoting electron transfer in semiconductors.[138]

3.3. Spin, chirality and life science

Efficient charge transfer is one of the important functions of living systems.[139] Electron transfer experiments in bR[126] and PSI[127] have verified the existence of CISS in animal and botanical systems. The correspondence between chirality and spin transfer provides the possibility of spin-guided electron transport in biomolecules, which plays an important role in redox reactions in biological systems and enantiomer specific recognition of chiral molecules,[82,140] becoming one of the main research directions of biophysics to explore electron transport related to CISS in organisms. Multiheme cytochromes are located on the surface of bacterial cells and are a long-distance electron transport channel connecting the inside and outside of cells, enabling microorganisms to obtain energy from redox minerals.[141] Using magnetic conducting probe AFM (Fig. 16(a)), Mishra *et al.*[141] found that electron transport through the extracellular conduits shows spin selectivity, and the SP of MtrF and OmcA was up to 37% and 63%, as shown in Fig. 16(b).

The net magnetic moment generated by spin is one of the sources of magnetism. Magnetic induction links magnetic fields to organisms. Different living things can sense different magnetic signals, including the angle, polarity and intensity. The phenomenon of birds, fish and turtles[142] using the geomagnetic field to sense the direction for migration and navigation has attracted the attention of scientists. Research studies that attempt to explain magnetic induction have been reported from the perspective of the CISS effect.[73,143] Banerjee-Ghosh *et al.*[132] reported that the interaction between chiral molecules and magnetic substrates is controlled by electron spin. To verify its universality in nature, selective adsorption of ds-DNA enantiomers has been studied. A fluorochrome was attached to ds-DNA. By measuring the fluorescence intensity of the Ni substrate at different adsorption times and in different

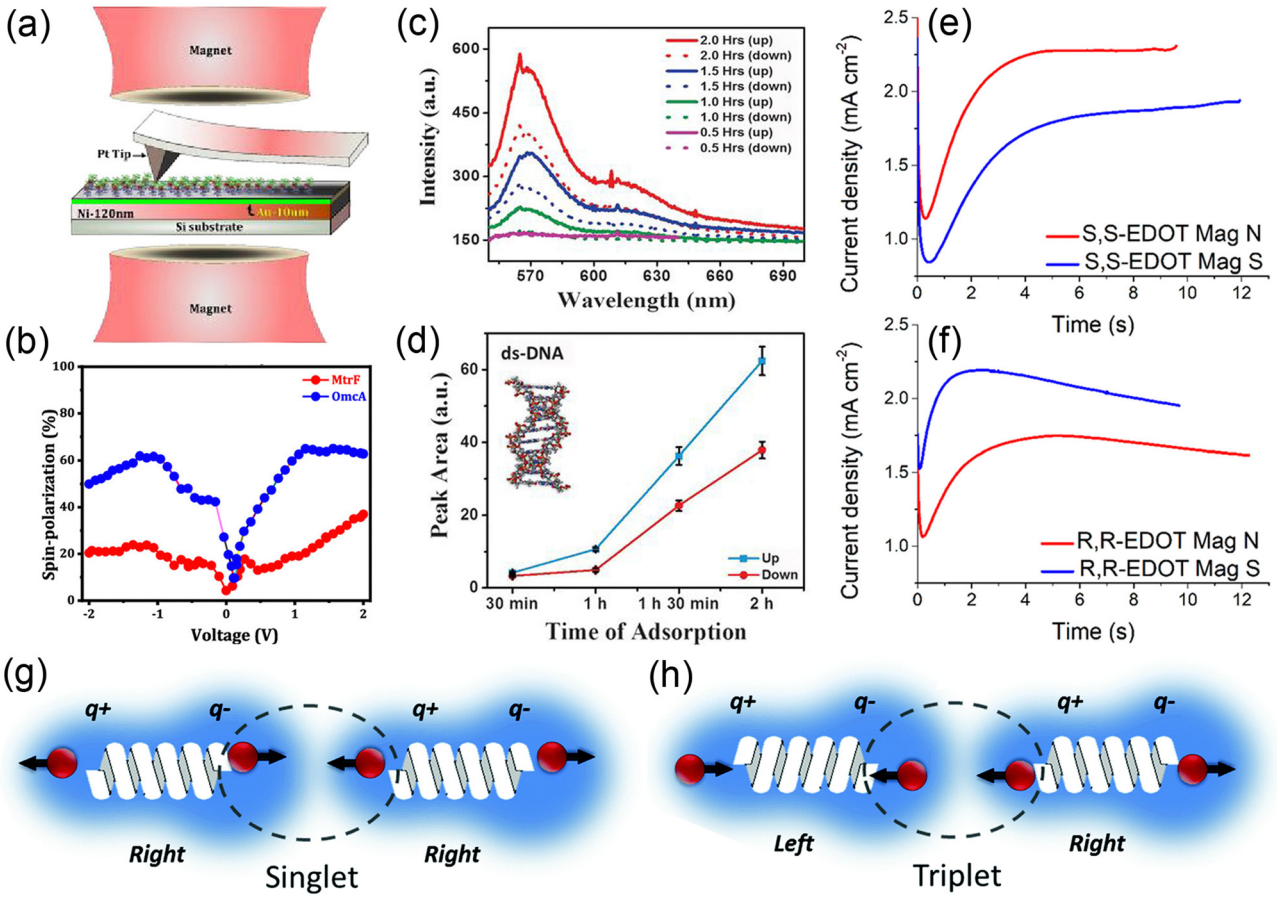

Fig. 16 (a) Scheme of the spin dependent conduction study measurement. (b) SP of MtrF and OmcA (two cytochromes) at different bias voltages. Reproduced with permission.[141] Copyright 2019©American Chemical Society. When the magnetic dipole of the substrate is pointing up (blue) or down (red), (c) fluorescence spectrum of ds-DNA adsorbed on a ferromagnetic substrate and (d) time dependence of the adsorption process. Reproduced with permission.[132] Copyright 2018©American Association for the Advancement of Science. Chronoamperometric studies of the electropolymerization of (e) *S,S*- and (f) *R,R*-EDOT using a ferromagnetic working electrode under the application of a north (red) and south (blue) magnetic field. Reproduced with permission.[144] Copyright 2020©American Chemical Society. Interaction between two helices with the (g) same and (h) opposite handedness. Reproduced with permission.[13] Copyright 2016 © Royal Society of Chemistry.

magnetic field directions, it was found that the substrate is more likely to bind to ds-DNA when the magnetic dipole direction is upward (Fig. 16(c) and (d)). Considering the experiment of self-assembled monofilms of polyalanine simulating biofilms, the adsorption converts the electric dipole to a magnetic dipole, which contributes to the magnetism of polyalanine films. Based on this, the disruptive view that biofilms may be magnetic was proposed.[108] Intracellular membrane structures, such as the nuclear membrane, endoplasmic reticulum and Golgi apparatus, play important roles in the recognition and transport of nucleic acids and proteins. If magnetic biofilms and spin selective adsorption between magnetic substrates and chiral enantiomers both exist, chiralilty- and spin-controlled enantiomer selective recognition and binding may be one of the mechanisms of macromolecular transport and protein synthesis in organisms. Fig. 16(e) and (f) shows the Ampere curve measured during the polymerization of chiral organic molecules on a ferromagnetic electrode, where the colors red and blue represent opposite electrode magnetization directions.[144] The change in current density over time can be divided into three processes. First, the current decreases due to the initial oxidation of monomers, and then the current increases with the increase in the oxidized monomers' concentration. Oligomers appear on the electrode surface as nucleation sites for the continuous growth of polymers. The slope of the current is proportional to the polymerization rate. Finally, polymer growth is restricted and the current reaches saturation. It can be seen that chirality and magnetization direction determine the rate of polymerization reaction, where the aggregation of *S*,*S*-diphenyl-3,4-ethylenedioxythiophene (EDOT) is faster under the application of a north magnetic field and *R*,*R*-EDOT aggregates faster under the application of a south magnetic field, suggesting that chiral molecular aggregation is affected by the magnetic field direction and verifying the corresponding relation between magnetism and chirality.[144]

The origin of life and chirality is a key topic in biophysics, which means the unification of physics and biology. The biological recognition process is an important part of biological processes. Michaeli *et al.*[13] proposed a recognition mechanism based on the CISS effect, which can enhance the interaction intensity between molecules with the same chirality. When the molecules are close enough, the electron clouds will overlap adequately so that the exchange interactions between molecules cannot be ignored. Here, we consider the electron cloud overlapping between two chiral helices. The SP of electron clouds in the overlapping region is antiparallel if the two helices have the same chirality, and parallel if the chirality is opposite. The interactions at the ends of chiral helices are analogous to those of hydrogen molecules containing two electrons, where each electron is bound to a proton. The electrons are degenerate when they are far enough apart, and are in the lowest energy level of hydrogen atoms. But when the electrons get close to each other, the Coulomb interactions make them to be non-degenerate states. According to the Pauli exclusion principle and indistinguishability of identical particles, electrons with opposite spin can transition between protons, which reduces the system energy by reducing the kinetic energy. Electrons with the same spin cannot transition between protons, so the system energy is relatively higher. Therefore, it can be inferred that helices with the same chirality are more conducive to the transport of electrons and lowering of system energy, which means that the same chiral molecules are more likely to connect into polymers. In organisms, the formation of polypeptides or nucleic acids depends on the aggregation of amino acids or nucleotides with the same chirality, which is consistent with the above deduction.

4. Chiral properties of hybrid organic inorganic perovskites

Chiral HOIPs were first reported by Billing *et al.* in 2003, in which the optical properties of traditional perovskites are combined with the spin selectivity of chiral materials.[145,146] Compared with biological macromolecules and inorganic QDs, chiral HOIPs have the advantages of adjustable band gaps, superior photoelectric performance and high spin selectivity.[147] HOIPs can be arranged into frames of different spatial dimensions by sharing halides in inorganic octahedra. By changing the layer number and chemical composition of metal halides, optical and electrical properties of two-dimensional (2D) HOIPs can be adjusted, which is beneficial in photoelectronic applications.[148]

4.1. Mechanism of chiral transfer

The mechanism of chiral transfer from chiral organic molecules to achiral inorganic components is an interesting topic in the field of HOIPs. To maximize the role of chiral HOIPs in spin dependent quantum transport, the origin and transfer mechanism of chiral activity must be clarified. At present, four phenomena have been shown to be related to chiral transfer in hybrid systems.[30]

Chiral surface distortion induced by chiral molecules. From the perspective of adsorption of chiral organic molecules on achiral inorganic surfaces, it can be considered that the structural distortion of inorganic surfaces is an effective way of chiral transfer. It was found that penicillamine[149] and chiral thiols[150] could strongly distort the surface of CdX (X = S, Se and Te) nanocrystals, transmitting chiral structures to the nanocrystal surface and associated electronic states, which successfully proved that chiral surface distortion can induce chiral activity in hybrid materials. In 2017, chiral distortion mediated by the interaction of chiral organic molecules and inorganic materials was first observed in chiral HOIPs. The $CsPb(I/Br)_3$ perovskite nanocrystals modified with chiral ligands showed obvious chiral activity in circular dichroism (CD) spectra, which remained unchanged even after the removal of chiral molecules.[151]

Chiral crystallization mediated by chiral molecules. Ben-Moshe *et al.*[152] proposed the concept of enantioselective chemistry based on the transformation of HgS from an achiral phase to a chiral phase, showing that chiral activity is mainly

contributed by chiral crystal structures. Ahn *et al.*[153] inserted *R*-MBA and *S*-MBA molecules into a layered lead iodide framework to obtain chiral HOIP crystal films, which exhibit the chiral space group of $P2_12_12_1$. However, when using racemic MBA for crystal preparation, the resulting (*rac*-MBA)$_2$PbI$_4$ perovskite has the inversion and mirror plane symmetry element of the achiral space group $P2_1/a$, which does not exhibit any chiral optical activity in the CD spectrum.

Supramolecular chiral self-assembly. Chiral ingredients on inorganic nanoparticle surfaces and amino acids lead to enantioselective interactions at interfaces, which in turn leads to the formation of highly distorted chiral helical morphology.[154] In 2018, through the supramolecular self-assembly method, Shi *et al.* found that achiral perovskite nanocrystals could coassemble with a chiral gelator, through which a new type of perovskite nanocrystal with circularly polarized luminescence was successfully prepared.[155]

Electronic interactions between chiral molecules and achiral frameworks. Coulomb dipole–dipole interaction can be used to transfer chirality from organic molecules to achiral inorganic frameworks.[156] By studying the photoelectric behavior of quasi 2D HOIP crystals with different organic spacer cations, it is found that the large π bond of the organic spacer plays a key role in the chiral transfer process, which can change the electronic configuration of the synthesized crystal through the coupling effect between the π-electron and p-orbital of iodide in the inorganic framework. This indicates that through the fine control of the electronic interaction between chiral organic molecules and achiral inorganic frameworks, it is possible to elucidate the origin of chiral transfer in HOIP systems.[157] By regulating the interaction of π electrons in chiral organic spacer cations, Ma *et al.*[158] systematically studied the influence of electronic interactions between chiral organic spacer cations and inorganic frameworks on the chiral activity of 2D HOIPs. The space of the templates with different nanopore sizes limits the growth of chiral HOIPs, which enables the precise control of the micro-strain in the 2D nanocrystals. The study indicates that chiral activity is influenced more by asymmetric hydrogen–bonding interaction between MBA and inorganic frameworks than the structural distortions of inorganic components, which plays an important role in promoting the chiral activity of HOIPs. Wang *et al.*[159] successfully synthesized six kinds of chiral antimony halide hybrids including four 0D edge-shared structures and two 1D corner-shared structures. Structural analysis shows that the organic ammonium cation distorts the antimony halide octahedron through asymmetric hydrogen-bonding interaction, transferring the chirality from organic sublattices to inorganic sublattices. The optical activity of chiral antimony halide hybrids is related to organic cations and structural dimensions, which can be understood through exciton coupling of dipole–dipole interactions. Controlling the electronic interaction between chiral organic molecules and inorganic frameworks becomes a key factor in designing high performance spin polarized optoelectronic devices.

Additionally, the chiral transfer mechanism was found to be strongly dependent on the number of chiral ligands.[151] When excess diaminocyclohexane is used to cover the surface of nanocrystals, chirality of perovskites is mainly caused by diaminocyclohexane gathering on the surface in a chiral pattern. In contrast, when the amount of diaminocyclohexane is low, the chiral characteristics are mainly caused by surface distortion and electron interaction. In conclusion, the origin and mechanism of chiral transfer in chiral perovskites largely depend on the crystal structure and synthesis method, which is very important for designing new chiral perovskites and improving the performance of corresponding photoelectric devices.[28]

4.2. Chiral optical behaviors

The photoluminescence response of $CH_3NH_3PbI_{3-x}Cl_x$ films was first explored, and the results are shown in Fig. 17(a) and (b).[160] The SP varies linearly with the magnetic field at a sample temperature of 18 K and decreases with an increase in sample temperature when the magnetic field is constant. Based on the structure of K_2NiF_4, 2D HOIPs were obtained by replacing K^+ with ammonium cations. When the number of inorganic layers was more than 1, quasi 2D chiral HOIPs evolved.[161] In 2018, Long *et al.*[29] achieved spin polarized photoluminescence characteristics in quasi 2D HOIPs through chirality transfer and energy funneling, as shown in Fig. 16(c)–(e). Chiral CD spectra show that low-dimensional perovskites have spin polarized photon absorption properties. In addition, due to the different emission rates of $\sigma+$ and $\sigma-$ polarization photoluminescence, a 3% SP photoluminescence can be observed even in the absence of an applied magnetic field. However, the spin polarized photoluminescence can only be achieved under an external magnetic field of 5 T for 3D achiral perovskites. SP varies linearly with the magnetic field intensity when the sample temperature is constant. In 2019, photoluminescence of 2D (*R*,*S*-methylbenzylamine)$_2$PbI$_4$ ((*R*,*S*-MBA)$_2$PbI$_4$) was reported, with an average SP of 9.6% and 10.1% for *R*- and *S*-type, respectively.[162] As shown in Fig. 17(f), the absolute value of SP of circularly polarized photoluminescence decreases with an increase in temperature. Kim *et al.*[163] investigated the effect of temperature on photoluminescence of (*R*,*S*-MBA)$_2$PbI$_4$ films, results of which were consistent with the reported conclusions,[105] as shown in Fig. 17(g). Long *et al.*[164] obtained all-dielectric perovskite metasurfaces from a planar nanostructure and found a spectral correspondence between the near- and far-field chirality. By adjusting the electric and magnetic multipole moments of resonant chiral supramolecules, a CD of 6350 mdeg and an anisotropy coefficient of up to 0.49 can be achieved. In addition, larger areas of metasurfaces can produce higher optical activity, which is close to the theoretical limit. In 2022, Ye *et al.*[165] studied the novel type-II core–shell nanocrystals, peripheral shells of which are composed of chiral perovskites and the central core is composed of 3D achiral $MAPbBr_3$. As shown in Fig. 18, there is spin dependent charge transport between the shell and core, which results in the spin polarized luminescence behavior of the combined type-II core–shell nanocrystals in the first excitation band of $MAPbBr_3$. This study provides evidence for the control of the CISS effect in type-II

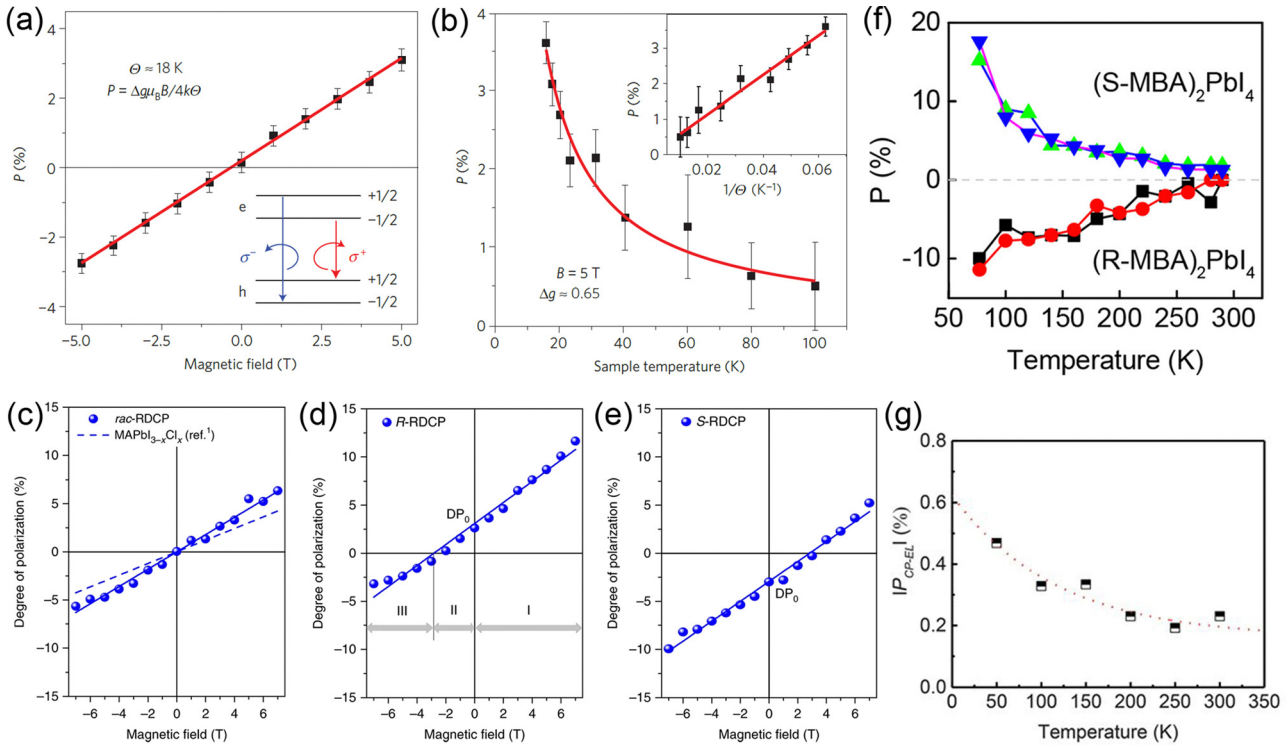

Fig. 17 Circular polarization, *P*, of $CH_3NH_3PbI_{3-x}Cl_x$ hybrid perovskites as a function of (a) applied magnetic field and (b) sample temperature. Reproduced with permission.[160] Copyright 2015©Springer Nature. Degree of photoluminescence polarization for (c) *racemic*- (d) *R*- and (e) *S*- reduced-dimensional chiral perovskites as the applied magnetic field varies from −7 T to 7 T. Reproduced with permission.[29] Copyright 2018©Springer Nature. (f) Degree of circularly polarized photoluminescence polarization as a function of temperature of two microplates for each type chiral $(MBA)_2PbI_4$ perovskites. Reproduced with permission.[162] Copyright 2019©American Chemical Society. (g) Temperature-dependent absolute average values of polarized photoluminescence polarization in light-emitting diodes based on $(S\text{-MBA})_2PbI_4/CsPbI_3$ CNCs. Reproduced with permission.[163] Copyright 2021©American Association for the Advancement of Science.

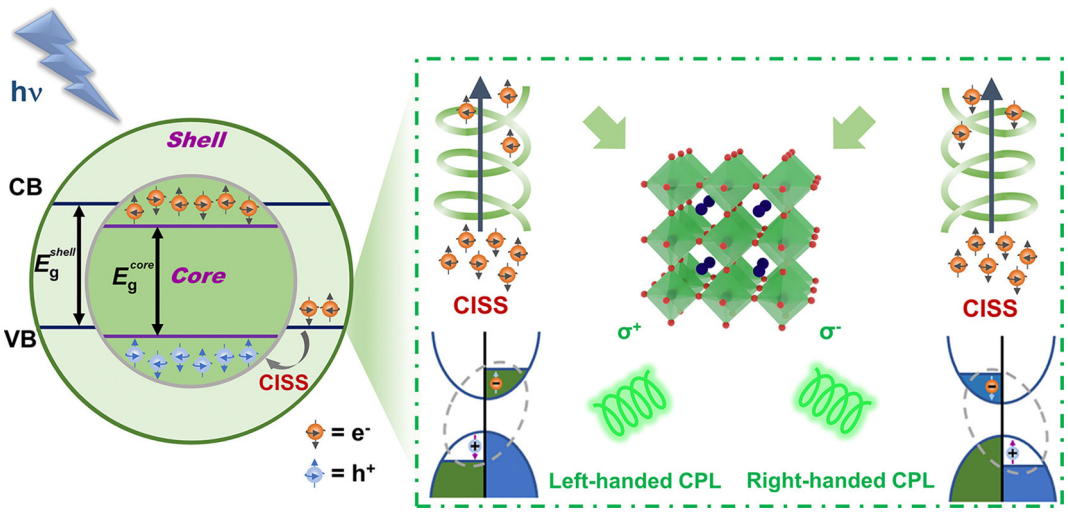

Fig. 18 Schematic illustration of spin polarized electron generation for circularly polarized luminescence in the core–shell nanocrystals. Reproduced with permission.[165] Copyright 2022©American Chemical Society.

core–shell nanocrystals and electron–hole recombination in the core, where the preferred spin state of transferred electrons is determined from the chiral shell. At room temperature, the photoluminescence quantum yield of type-II core–shell nanocrystal films is up to 54%. Additionally, nontoxic block-like $(R,S\text{-NEA})_2CuCl_4$ and needle-like $(R,S\text{-CYHEA})_6Cu_3Cl_{12}$ single crystals were synthesized in 2023, exhibiting chiral CD signals.[166]

4.3. Spin selective electron transfer

Strong SOC, long spin relaxation time, tunable Rashba splitting and chirality lead to highly spin-dependent properties resulting from the CISS effect, which is mainly reflected in two physical processes in HOIPs, including the magneto-optical Kerr effect and spin dependent charge transport processes. Magneto-optical detection results based on 2D HOIPs are shown in Fig. 19(a)–(c).[102] Under light illumination, the Kerr signal of achiral samples does not change significantly, but decreases and increases under S-HOIP/NiFe and R-HOIP/NiFe conditions, respectively. When the magnetic field reverses, the Kerr signal also reverses, suggesting that chirality dependent spin polarized photocurrents are generated in chiral HOIPs under photoexcitation, which can be regulated by an external magnetic field. In 2023, based on the time-resolved magneto-optical Kerr effect and 2D HOIPs, Kim *et al.*[167] investigated the transient spin current generated by chiral phonons in adjacent non-magnetic conductors. The phase and magnitude of the spin current are strongly dependent on the chirality and external magnetic field, which means that the electron spin–phonon coupling at the interface is driven by a thermal gradient. Charge transport in 2D chiral lead iodide perovskites was investigated using magnetic conductive probe AFM, from which it was found that hybrid system exhibits spin selective effects caused by the spin polarized tunneling barrier of organic components.[33] Fig. 19(d) shows the CD spectra of R,S-HOIP films, where the peaks with opposite symbols indicate different preferences of chiral HOIPs for circularly polarized light.[33] High energy CD signals are derived from the optical activity of organic molecules, while low energy CD response is derived from the induced optical activity of inorganic frames, which provides direct evidence for the induced chirality of inorganic components. When the carriers pass through a film with a thickness of 50 nm, they cross 36 chiral potentials composed of organic–inorganic layers, where the maximum SP is up to 86%, indicating that multiple chiral tunneling processes can improve the efficiency of spin selectivity. In addition, this experiment verifies the weak dependence of SP on film thickness, indicating that spin selectivity saturates in a few tunneling processes and thicker films cannot induce higher SP.

Although the spin filtering ability of $(R,S\text{-MBA})_2PbI_4$ has been demonstrated, the hazards of lead to the human body and environment limit the application of lead based perovskites. Lu *et al.*[168] studied the vertical electronic transport through $(R,S\text{-MBA})_2SnI_4$ perovskites (50–60 nm), which are shown in Fig. 20(a) and (b). Compared to $(S\text{-MBA})_2SnI_4$, the current in $(R\text{-MBA})_2SnI_4$ is larger when the magnetization direction is upward and smaller when the magnetization direction is downward. Under a bias voltage of −1 V, the SP of $(R\text{-MBA})_2SnI_4$ and $(S\text{-MBA})_2SnI_4$ perovskites is 94% and −93%, respectively, which is the same as that of lead based perovskites. In addition to the toxicity of cations within an inorganic framework, the stability of anions has also attracted much attention. The inherent oxidation tendency of I^- brings hidden dangers to the stability and useful life of electronic devices. Lu *et al.*[169] synthesized 1D chiral $(R,S\text{-MBA})PbBr_3$ by a

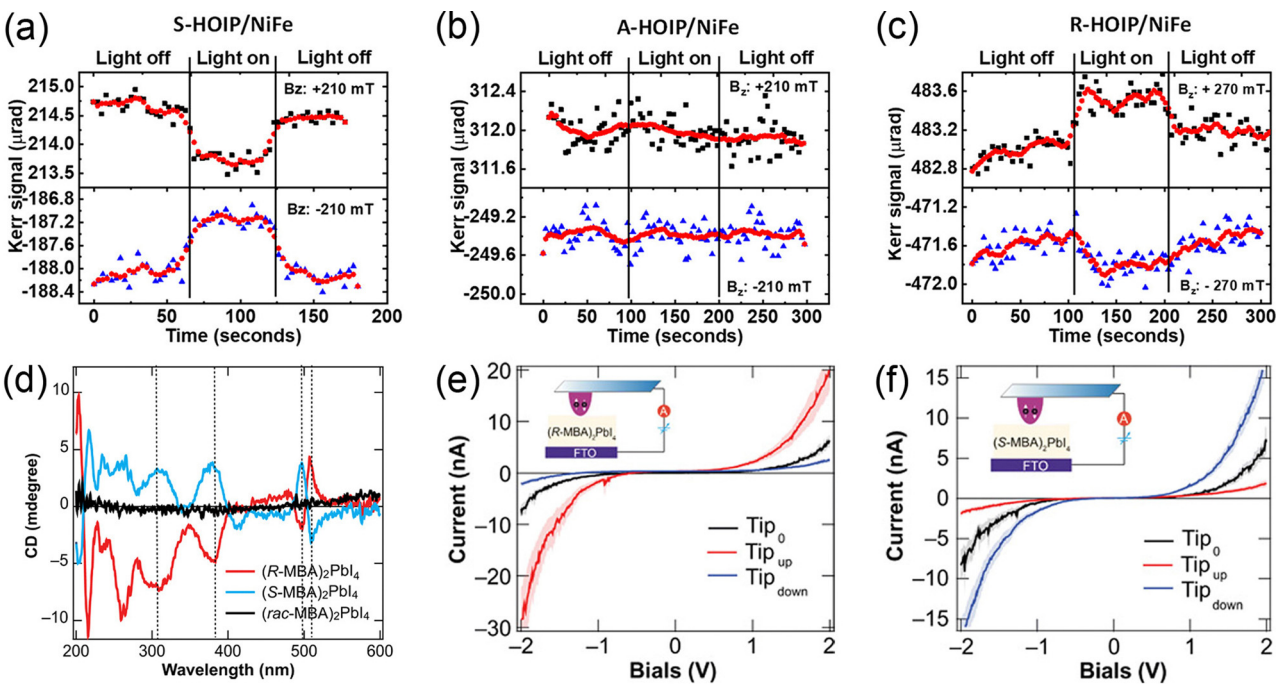

Fig. 19 The change in Kerr signals for (a) S-HOIP/NiFe, (b) achiral-HOIP/NiFe and (c) R-HOIP/NiFe under photoexcitation, when the samples are placed in an out-of-plane magnetic field. Reproduced with permission.[102] Copyright 2020©American Chemical Society. (d) CD spectra display derivative features at 200 to 600 nm, where $(R\text{-MBA})_2PbI_4$ and $(S\text{-MBA})_2PbI_4$ exhibit opposite signs. The room-temperature I–V curves of (e) $(R\text{-MBA})_2PbI_4$ and (f) $(S\text{-MBA})_2PbI_4$ obtained by magnetic conductive probe AFM, where the tip is magnetized in the north (blue) and south (red), and nonmagnetized (black). Reproduced with permission.[33] Copyright 2019©American Association for the Advancement of Science.

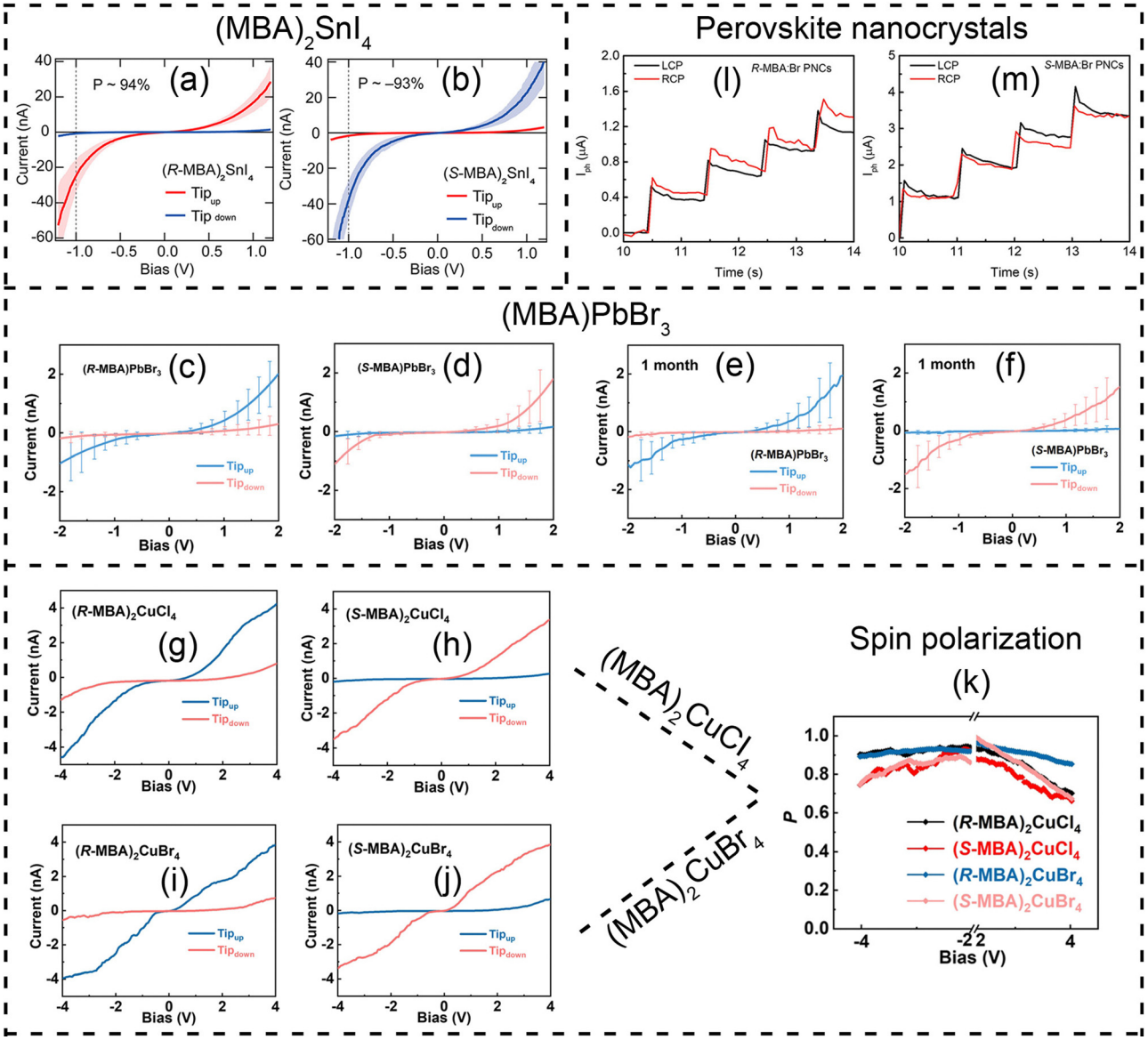

Fig. 20 *I*–*V* curves of (a) (*R*-MBA)$_2$SnI$_4$ and (b) (*S*-MBA)$_2$SnI$_4$ films obtained by magnetic conductive probe AFM at room temperature. Reproduced with permission.[168] Copyright 2020©American Chemical Society. *I*–*V* curves of (c) (*R*-MBA)PbBr$_3$ and (d) (*S*-MBA)PbBr$_3$ films. (e), (f) Stability test of chiral (MBA)PbBr$_3$ films. Spin-dependent charge transport of (e) (*R*-MBA)PbBr$_3$ and (f) (*S*-MBA)PbBr$_3$ films obtained after 1 month using magnetic conductive probe AFM, where the probe is magnetized in the up (blue) and down (red) directions. Reproduced with permission.[169] Copyright 2020©John Wiley and Sons. The *I*–*V* curves of (g) (*R*-MBA)$_2$CuCl$_4$, (h) (*S*-MBA)$_2$CuCl$_4$, (i) (*R*-MBA)$_2$CuBr$_4$ and (j) (*S*-MBA)$_2$CuBr$_4$ films at room temperature when the probe is magnetized in the upward (blue) and downward (red) directions. Bias dependent SP of (k) (*R*/*S*-MBA)$_2$CuX$_4$ (X = Br, Cl) films. Reproduced with permission.[170] Copyright 2021©John Wiley and Sons. Time dependent photocurrent variations of circularly polarized light detectors based on (l) *R*- and (m) *S*-perovskite CNC/SWCNT heterojunctions. Reproduced with permission.[174] Copyright 2022©John Wiley and Sons.

cooling crystallization method. Compared with 2D (*R*,*S*-MBA)$_2$PbI$_4$, (*R*,*S*-MBA)PbBr$_3$ has higher stability and durability to oxygen, humidity and temperature. The measurement results of magnetic conductive probe AFM are shown in Fig. 20(c)–(f).[169] The spin filtering efficiency of (*R*,*S*-MBA)PbBr$_3$ is up to 90%, which shows no significant attenuation after 1 month, proving the great spin filtering ability of highly stable hybrid perovskites and providing an important support for expanding the application range of spintronic devices. Chiral (*R*,*S*-MBA)$_2$CuX$_4$ (X = Cl and Br) combines the low toxicity of Cu^{2+} with the stability of Cl^- and Br^-, and is a kind of environmental friendly and stable material. Experimental charge transport results of (*R*,*S*-MBA)$_2$CuX$_4$ (X = Cl, Br) are shown in Fig. 20(g)–(k).[170] The *R*-Type perovskite tends to transport spin-up electrons, while the *S*-type perovskite tends to transport spin-down electrons. Under a bias voltage of ±2 V, spin filtering efficiency is up to 90%. In addition, the spin filtering efficiency decreases with an increase in voltage. Due to the complex structure of low-dimensional chiral perovskite crystals, it is still a great challenge to obtain films with low roughness. In 2022, chiral metal halide crystals of (*R*,*S*-NEA)$_2$CoCl$_4$ were successfully prepared, in which the stable CH–π interaction enables strong film forming ability.[171]

The CISS efficiency is up to 90%. By adding a tiny amount of Alq3 to NEA, an ultrasmooth film with a roughness of 0.3 nm can be obtained. In addition, Wei *et al.*[172] studied the spin properties of lead based chiral HOIPs through the first principles calculations, and found that halogen substitution can significantly improve the value of spin splitting of chiral molecules. Compared with the condition without substituting halogens (13 meV), the spin splitting values after substituting F, Cl and Br are increased to 73, 90 and 105 meV, respectively. Calculations show that halogen substitution has a strong modification effect on the electrostatic potential surface of chiral molecules.

In conclusion, chiral HOIPs exhibit strong SOC, ferroelectricity, Rashba spin splitting, unique optical selectivity and spin selective charge transfer, and are an important candidate for photovoltaic materials and spintronics devices.[173] By changing the layers and chemical composition of inorganic metal halides, the optical and spin selective electronic properties of 2D chiral HOIPs can be adjusted. Organic ligands and inorganic frameworks provide the sources of chirality and SOC, respectively, and can regulate the structure and properties of chiral perovskites through interactions. Through the theoretical calculation which simulates heterostructures composed of perovskite CNCs and SWCNTs illuminated with circularly polarized light, it is found that heterostructures containing *R*-type perovskite CNCs show higher photocurrent when excited with right-handed circularly polarized light, while heterostructures containing *S*-type perovskite CNCs show higher photocurrent when excited with left-handed circularly polarized light, as shown in Fig. 20(l) and (m). This experimental result shows that perovskite CNCs can be used as a detector of circularly polarized light.[174] Besides HOIPs, hybrid organic inorganic materials, such as helical metal peptide,[175] chiral helical metal–organic frameworks,[176] chiral molecules and metal cation complexes,[177] chiral bioorganic crystals[178] and chiral molecular intercalation superlattices,[179,180] have also attracted the attention of researchers. Chiral manipulation of electron spin will provide a new strategy for the development of spintronics.

5. Spin selectivity in chiral inorganic materials

Studying the formation of asymmetrical morphology in crystalline structures is an important step to understand the natural chirality.[181] Inorganic materials have the characteristics of hardness, high temperature resistance, corrosion resistance and oxidation resistance, and have broad application prospects in modern industry, national defense and life. The CISS effect has been demonstrated in three types of inorganic materials, namely, chiral inorganic crystals, chiral oxides and chiral nanoparticles.

5.1. Crystals

Current induced magnetization of uniaxial chiral $CrNb_3S_6$ crystals was explored through a superconducting quantum interference device, the lattice structure and experimental setup of which are shown in Fig. 21(a) and (b).[182] The results (Fig. 21(c) and (d)) show that the *M*–*H* curve is shifted by the application of current, which determines the translation direction of the *M*–*H* curve. In order to exclude the effect of Joule heat on the curve shift, the magnetization contributed by the CISS effect (ΔM_{even}) is defined as $\Delta M_{even} = \frac{[M_{(+H)} + M_{(-H)}]}{2}$, which only appears when the current is nonzero. The symbol of

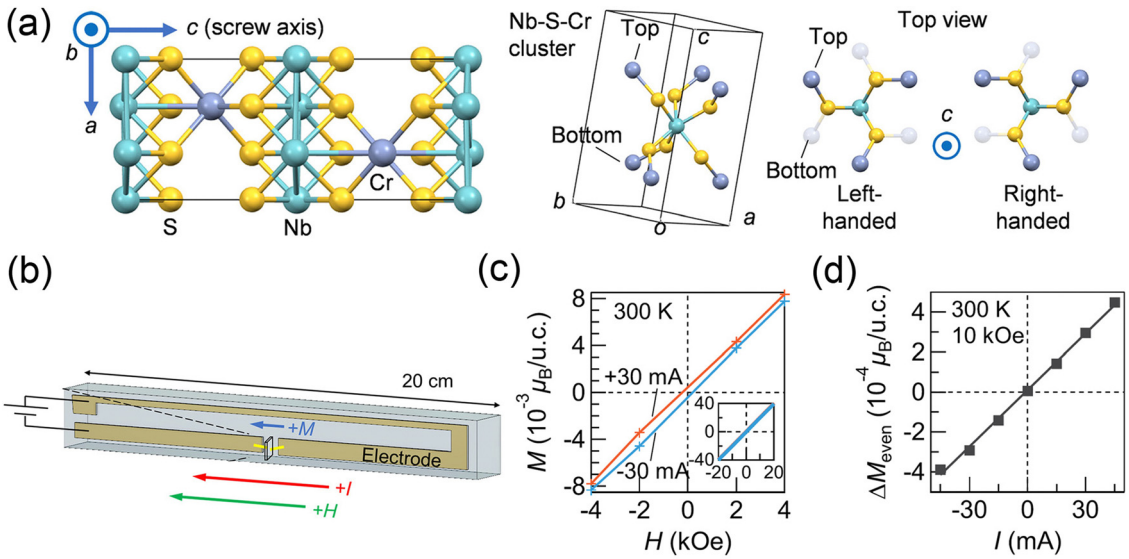

Fig. 21 (a) Crystal structure of $CrNb_3S_6$. (b) Diagram of the experimental measuring device. (c) *M*–*H* curves in the range of ±4 kOe for *I* = 30 and −30 mA. The inset shows *M*–*H* curves in the range of ±30 kOe. (d) Current dependence of ΔM_{even} at *H* = 10 kOe. Reproduced with permission.[182] Copyright 2020©AIP Publishing.

ΔM_{even} is related to the current direction and the magnetization intensity induced by current changes linearly with the current magnitude in chiral systems. Inui *et al.*[183] studied the spin transport characteristics of uniaxial chiral $CrNb_3S_6$ under zero magnetic field at room temperature, which involved three devices with the electrode thicknesses of 6, 9 and 20 nm,. The chirality of device 3 was different from that of device 1 and device 2. The experimental results are shown in Fig. 22(c) and (d), where the absolute value of the curve slope decreases with the increase in electrode thickness and the SP can be controlled by changing the current direction and crystal chirality. Besides the signal of the CISS effect, the signal of inverse CISS (ICISS) was detected in the same device containing chiral $CrNb_3S_6$, confirming the reciprocal relationship of CISS phenomenon, which was also demonstrated in the polycrystalline samples of chiral $NbSi_2$ and $TaSi_2$. In order to further explore the CISS effect in bulk $NbSi_2$ and $TaSi_2$ polycrystalline samples, Shishido *et al.*[184] conducted position dependent experiments, results of which are shown in Fig. 22(g)–(j). Spin polarized signals in non-local measurements indicate that spin polarized phenomenon occurs regardless of the presence of crystalline grain. The results demonstrate the robustness of the CISS effect, and also show that the spin transmission ability over long distances of chiral crystals is independent of crystallinity. In inorganic crystals, long distance spin transport occurs over a distance of more than 10 μm.[185] Furukawa *et al.*[186,187] reported the phenomenon of current induced magnetization of Te, and pointed out that this phenomenon was attributed to band splitting caused by broken inversion symmetry. Subsequently, the phenomenon of current induced magnetization has been linked to the CISS effect and the displacement of the nuclear magnetic resonance spectrum under pulse current is measured experimentally. Induced magnetization can be parallel to applied current according to the chirality of Te, which is in contrast to the induced magnetization perpendicular to applied current related to the Rashba effect. Diode effects refer to the phenomenon that carriers can only migrate in one direction and not in the opposite direction. In 2022, Chen *et al.*[188] revealed the relationship between chiral structures and phonon excitation, demonstrating the chiral phonon diode effect in chiral crystals. At a certain frequency, phonons with certain chirality can only propagate in one direction and not in the opposite direction.

5.2. Oxides

Photo-electro-chemical water decomposition is a promising method for hydrogen production, where the CISS effect plays an important role in improving the efficiency. For example,

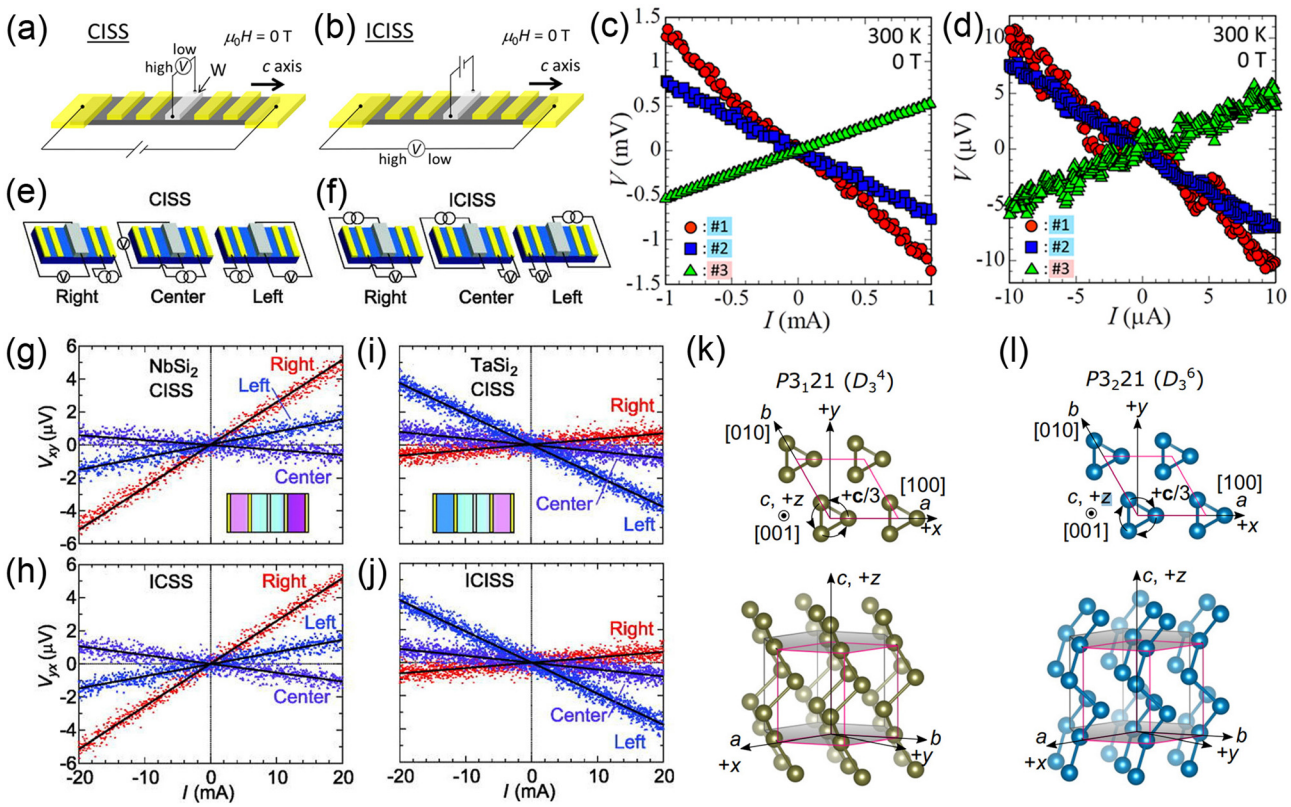

Fig. 22 Experimental measurement devices for (a) CISS and (b) ICISS effect. *I*–*V* characteristics of (c) CISS and (d) ICISS at 300 K at 0 T are provided. Reproduced with permission.[183] Copyright 2020©American Physical Society. Setups for location-sensitive measurements of (e) CISS and (f) ICISS in $NbSi_2$ and $TaSi_2$ polycrystals. The *I*–*V* characteristic curves of (g), (h) $NbSi_2$ and (i), (j) $TaSi_2$ polycrystals at room temperature. Reproduced with permission.[184] Copyright 2021©AIP Publishing. Crystal structures of (k) right-handed and (l) left-handed triangular Te. Reproduced with permission.[187] Copyright 2021©American Physical Society.

inorganic electrodes wrapped with chiral molecules can improve the hydrogen production and reduce by-product generation.[189,190] According to the available reports,[15,84,90,115] the spin filtering ability of organic molecules is highly dependent on their spatial structure, which leads to the decline of SP in extreme environments (such as low temperature, high temperature, high acidic and strong alkali, *etc.*) and restricts the stability of their spin filtering efficiency. Chiral CuO is a typical chiral inorganic oxide. In the early 21st century, chiral CuO was successfully prepared based on electrochemical deposition, chirality of which was determined from the chiral precursors.[191,192] In 2019, Ghosh *et al.*[193] reported the spin selectivity phenomenon of chiral CuO films and found its ability of improving efficiency in photo-electro-chemical water decomposition. The results show that SP of photoelectrons of CuO films deposited on Au substrates increases with the increasing thickness of CuO films and reaches saturation when the film thickness is about 30 nm, as shown in Fig. 23(a). Compared with achiral CuO, chiral CuO reduced the overpotential, and significantly inhibited the generation of H_2O_2 as a by-product, making an important step in the field of inorganic materials with spin filtering ability. Zhang *et al.*[194] deposited chiral CuO films on foam Ni through the electrolyte of chiral tartaric acid, where the CuO films prepared with L-tartaric acid were named L-CuO and those prepared with D-tartaric acid were named D-CuO. It is found that chiral CuO has a catalytic effect on the water decomposition process, where the 3D continuous macroporous frame provides a large reaction area and allows better permeation of electrolyte. As shown in Fig. 23(b) and (c), in the electrolyte containing L-tartaric acid, L-Cuo/Ni exhibits higher current density and lower reduction potential, while D-Cuo/Ni shows opposite characteristics, which indicates that L-CuO/Ni and D-CuO/Ni show opposite response related to chirality. In 2020, Ghosh *et al.*[195] explored the application of chiral cobalt oxide thin film electrocatalysts in the oxygen evolution reaction. The spin polarized charge

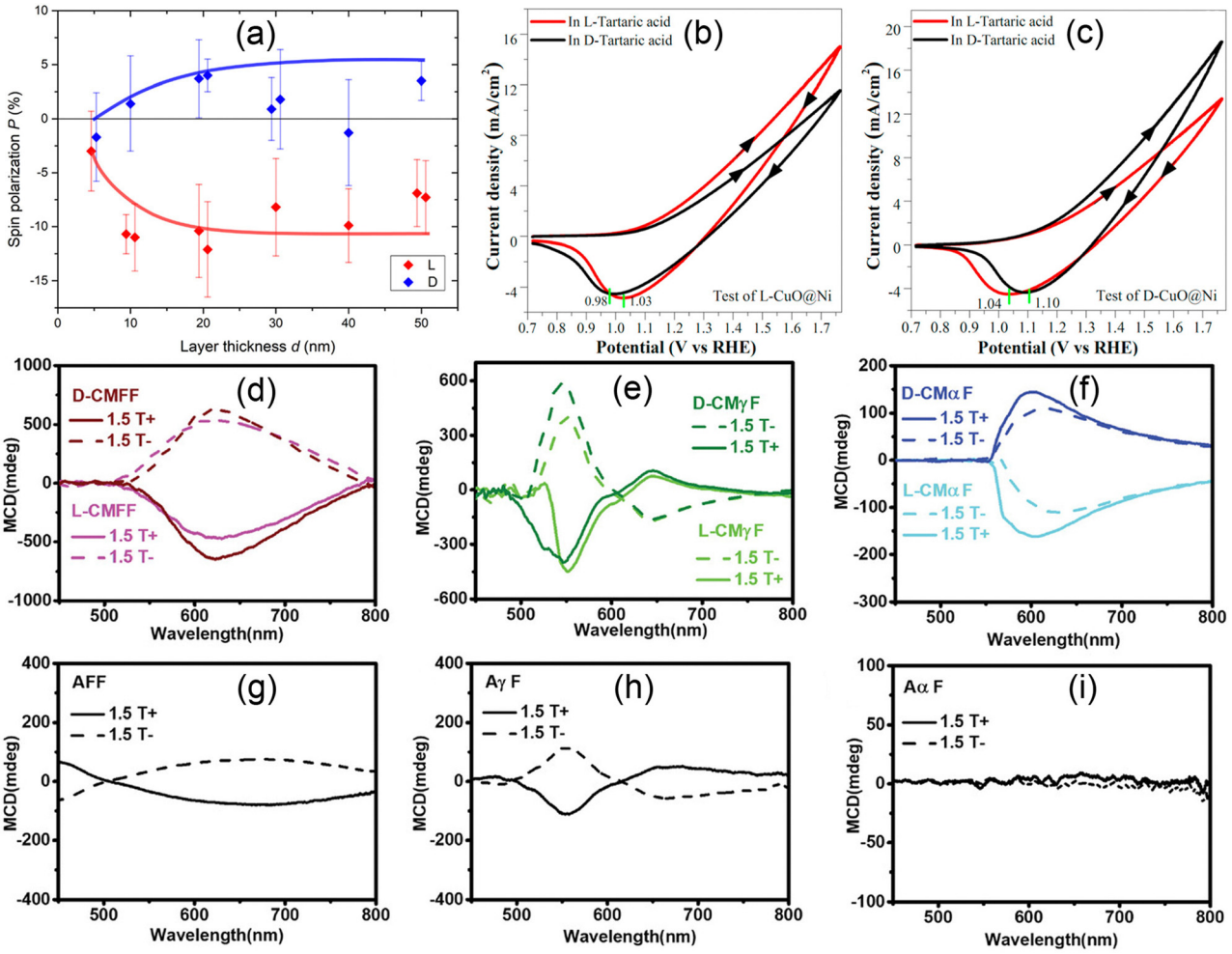

Fig. 23 (a) SP of the photoelectrons in the Au/CuO films varies with the thickness *d* and chirality. Reproduced with permission.[193] Copyright 2019©American Chemical Society. Electrochemical selectivity test of the surface of (b) L-CuO@Ni and (c) D-CuO@Ni at room temperature. Reproduced with permission.[194] Copyright 2021©Elsevier. Under parallel (solid lines) and antiparallel (dashed lines) magnetic fields, magnetic CD spectra of (d) chiral CMFF, (e) chiral CMγF, (f) chiral CMαF, (g) achiral Fe_3O_4 (AFF), (h) achiral γ-Fe_2O_3 (AγF) and (i) achiral α-Fe_2O_3 (AαF). Reproduced with permission.[196] Copyright 2022©John Wiley and Sons.

transfer generated by the CISS effect plays an important role in the process of reducing overpotential and increasing oxygen production.

Chiral mesostructured Fe_3O_4 (CMFFs), mesostructured γ-Fe_2O_3 (CMγFs) and mesostructured α-Fe_2O_3 (CMαFs) films were prepared by the calcination method, experimental results of which are shown in Fig. 23(d)–(i).[196] Ferromagnetic CMFFs and CMγFs show magnetism dependent CD spectra, while antiferromagnetic CMαFs show chirality dependent CD spectra, from which it is speculated that the competition between effective magnetic field induced by spin and chiral determines the energy splitting of opposite spins in different magnetic materials. In 2021, chiral mesostructured NiO films were successfully prepared through the symmetry breaking effect of chiral molecules, including primary nanoflakes with atomically twisted crystal lattices and secondary helical stacked nanoflakes.[197] The results of magnetic conductive probe AFM and magnetic CD confirm the CISS effect of chiral mesostructured NiO films.

5.3. Nanoparticles

In addition to inorganic crystals and oxides, new progress related to the CISS effect has been made in helical nanowires. The spin dependent band structure and spin transport of chiral Au nanotubes were calculated by the relativistic linearized augmented column cylindrical wave method, which showed that the chiral induced spin polarized electron transport of inorganic chiral Au nanotubes can be controlled by torsion, stretching and compression.[198] Based on the principles of quantum mechanics, spin dependent electron transport in chiral inorganic SnIP helical nanowires is derived through a tight binding model,[199] which shows that the mobility of electrons in axially chiral structures depends on the direction of spin angular momentum, velocity direction and the structural chirality. Fig. 24 shows the electron transport properties of chiral SnIP nanowires, where M and P denote SnIP nanowires with left-handed and right-handed helices, CW and CCW denote wave packet propagation along CW or CCW. For electrons with spin parallel (antiparallel) to the *z*-axis in M-SnIP nanowire, the CW (CCW) direction wave packet generates a faster probabilistic current, while the P-SnIP nanowire shows

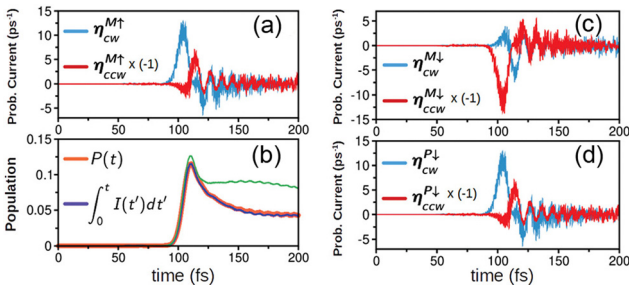

Fig. 24 Electron transport properties in chiral SnIP nanowires, M and P denote SnIP nanowires with left-handed and right-handed helices, CW and CCW denote wave packet propagation along CW or CCW, and ↑ and ↑ denote spin parallel or antiparallel to the *z*-axis. Reprinted with permission.[199] Copyright 2021©American Chemical Society.

the opposite behavior. Additionally, in 2022, Liu *et al.*[200] found that chiral antipodal nanostructured Au films exhibited photomagnetic-chiral anisotropy, where the opposite photomagnetic fields were generated under unpolarized irradiation. This effect is induced by the effective magnetic field generated by the electron movement in opposite chiral helices, overcoming the limitation that precious metals lacking SP cannot be used as photoelectric materials.

6. Summary and future prospects

In this paper, we summarize the important findings during the development of the CISS effect. According to the organic and inorganic properties of materials, progress of spin polarized transport in various types of materials is reviewed, where the mechanisms, experimental techniques and biological significance of the CISS effect are also discussed. There are various reported experimental conditions, substrate types, material properties and observation methods of the CISS effect, but they still reveal some rules and characteristics of spin polarized transport in chiral systems. When electrons move in chiral molecules, the spin direction tends to be parallel or antiparallel to the electron velocity direction. Generally, SP of charge transfer increases with the increase in applied voltage in chiral organic materials. In a specified temperature range, SP of oligopeptide rises with the increasing temperature. Extreme environments, such as high temperature, strong acid and strong alkali, damage the spatial structure of oligopeptides, denaturing them and making them lose their spin filtering ability. In addition, within the scope of a certain length, SP is proportional to the length of chiral molecule or helices, indicating that multiple tunneling processes can improve the efficiency of spin selectivity. It is worth noting that the SP does not grow linearly with the length of chiral structures, but reaches saturation after certain tunneling processes. Light, humidity, chirality and magnetic field are also the factors influencing the CISS effect, and their interactions have become the key to breakthroughs in the development of life science and spintronics. The spin filtering ability of different chiral systems may be strengthened or weakened under light illumination, which is related to the optical sensitivity of chiral molecules. Structure-dependent charge transport in chiral systems shows that stress can effectively regulate the spin filtering ability of chiral materials, which declines with an increase in compressive stress. The relationship between spin filtering and stress shows that SOC is enhanced by longitudinal stretching and weakened by compression.

The CISS effect is a promising driving force in spintronics, making remarkable contributions in the fields of optics,[42] chemistry,[201,202] biology[203] and quantum nanodevices.[204–207] The magnetoresistance of chiral devices has also attracted the attention of researchers.[208,209] Compared with ferromagnets, chiral structures have the advantages of high SP, excellent interface, simple preparation process and low cost, which can help get rid of ferromagnetic electrodes and achieve efficient

spin injection.[210] The application of the CISS effect in the field of spintronics has successfully reduced magnetoresistive random access memory from micron to a nanometer scale,[132] which can endow spintronic devices with interesting properties including electroluminescence and high absorbance,[211] demonstrating the advantages of the CISS effect in designing electronic devices. On GaAs/AlGaAs heterostructures covered with chiral self-assembled monolayers, a submicron scale local magnetic field can be generated at room temperature by applying a bias voltage of 0.1 V.[88] Interactions between electron spin, magnetic field and polarized light show the spin filtering ability of chiral biological systems,[126,127] which provides a new exploration direction for life science. At present, flexible application of the CISS effect to life science and practical spintronic devices is still a long way off. Several future directions and problems concerning CISS effect are discussed here.

(i) Based on the reports on the CISS effect, unconventional SOC plays an important role in finding materials with high spin filtering ability, sources of which are usually considered as helical structures, electronic correlation and lattice vibration. It has recently been reported that the CISS effect does not depend on the helical structure.[212] The exploration of mechanism provides an important opportunity for the development of the CISS effect.

(ii) The research on spin polarized transport of chiral organic molecules has laid a good foundation for the development of the CISS effect. The induction of SP in conductive materials by helical functionalization of specific bps is an interesting direction for the development of the CISS effect, but the underlying mechanism and influence of specific bp on SP remain unclear. In addition, the spin polarized transport process of RNA associated with the CISS effect has not been reported.

(iii) The CISS effect of organic molecules is mainly studied in biological macromolecules. The spin selective characteristics of lactic acid and other small chiral molecules has not been reported. Studies on the spin polarized transport of amino acids have focused on a few amino acids, such as cysteine, alanine and proline. The spin transport processes of other amino acids are still unclear.

(iv) The experiment using self-assembled monolayers of polyalanine peptides to simulate biofilms predicts the advantages of the CISS effect in life process, which establishes a good connection between the CISS effect and living systems. Enantioselective binding between chiral molecules and magnetic substrates based on the CISS effect is expected to improve the accuracy of biometric recognition, but it still faces many difficulties in device manufacturing and practical application. Enantioselective recognition in organisms controlled by chirality and spin may be one of the mechanisms involved in macromolecular transport and protein synthesis, and how the CISS effect controls recognition during life remains an interesting question.

(v) The research fields involving chiral hybrid organic inorganic materials and spin selective transport of inorganic materials are still in a fledging period. Spin polarized transport processes and regulation under light, magnetic field, electric field and stress are still unclear in most materials.

(vi) The combination of chiral and inorganic is an attractive emerging field. Chiral HOIPs open the door to introducing organic chirality into inorganic frameworks. Is it possible to introduce inorganic chirality into organic materials? In addition, composite structures are beneficial to obtain high SP, such as the combination of ss-DNA and SWCNTs. Based on the structure of ss-DNA hybrid SWCNTs, what interesting phenomena will be observed when the achiral carbon nanotubes are replaced with chiral Au nanowires or SnIP nanowires?

(vii) Spin polarized current generated by chiral materials can be well maintained in achiral molecular wires, indicating that chiral structures are not necessary for spin current conduction. In the further propagating processes of spin polarized current in achiral structures, how to reduce current loss and increase transmission length is the focus in this research direction. In addition, it is necessary to propose and develop a more general preparation method in the field of chiral–achiral composite material preparation that can solve the shortcomings of current transfer technology.

(viii) By changing the layers and chemical composition of inorganic metal halides, the optical and spin selective electronic properties of 2D chiral HOIPs can be adjusted. Non-toxic lead-free hybrid materials with high stability are urgently needed for spin filtering in designing spintronics devices. Therefore, the toxicity of metal cations and the stability of halogenated anions have attracted researchers' attention, and searching for environmentally friendly, stable and efficient chiral HOIPs has become a new development direction.

(ix) Studies linking chirality to Dzyaloshinskii–Moriya interaction are still in infancy. The polarization sign of electron transport through helical magnets depends on the chirality of helices. SP increases with the increase in the Dzyaloshinskii–Moriya interaction strength.[213] At present, switches of magnetization based on Dzyaloshinskii–Moriya interaction have been reported.[214] The relationship between Dzyaloshinskii–Moriya interaction and spin filtering ability in chiral helical magnets remains to be further explored.

(x) Chiral topological quantum materials, such as chiral topological insulators and chiral Weyl semimetals, can generate large spin currents that are used to drive the spin–orbit torque, which can effectively move chiral domain walls and magnetic skyrmions, effectively demonstrating the huge charge-spin conversion efficiency of the spin–orbit torque devices.[215] Combining the CISS effect with topological quantum matter is an interesting field for developing novel materials.

Conflicts of interest

There are no conflicts of interest to declare.

Acknowledgements

This work is supported by the National Natural Science Foundation of China (52071233).

References

1 S. H. Yang, *Appl. Phys. Lett.*, 2020, **116**, 120502.
2 R. Naaman, *Isr. J. Chem.*, 2016, **56**, 1010–1015.
3 V. Dediu, M. Murgia and F. C. Matacotta, *Solid State Commun.*, 2002, **122**, 181–184.
4 Z. H. Xiong, D. Wu and Z. V. Vardeny, *Nature*, 2004, **427**, 821–824.
5 K. V. Raman, S. M. Watson, J. H. Shim, J. A. Borchers, J. Chang and J. S. Moodera, *Phys. Rev. B: Condens. Matter Mater. Phys.*, 2009, **80**, 195212.
6 S. F. Mason and G. E. Tranter, *Mol. Phys.*, 1984, **53**, 1091–1111.
7 W. Q. Wang, *Wuli*, 1994, **23**, 116–120 (in Chinese).
8 W. Q. Wang and X. R. Sheng, *Shengming Kexue*, 1995, **7**, 40–41 (in Chinese).
9 K. Ray, S. P. Ananthavel, D. H. Waldeck and R. Naaman, *Science*, 1999, **283**, 814–816.
10 B. Göhler, V. Hamelbeck, T. Z. Markus, M. Kettner, G. F. Hanne, Z. Vager, R. Naaman and H. Zacharias, *Science*, 2011, **331**, 894–897.
11 K. M. Alam and S. Pramanik, *Adv. Funct. Mater.*, 2015, **25**, 3210–3218.
12 D. M. Sterner, J. M. Abendroth, K. M. Cheung, M. Ye, M. S. El Hadri, E. E. Fullerton and P. S. Weiss, *Nano Lett.*, 2020, **20**, 1218–1225.
13 K. Michaeli, N. Kantor-Uriel, R. Naaman and D. H. Waldeck, *Chem. Soc. Rev.*, 2016, **45**, 6478–6487.
14 A. C. Aragonès, E. Medina, M. Ferrer-Huerta, N. Gimeno, M. Teixido, J. L. Palma, N. J. Tao, J. M. Ugalde, E. Giralt, I. Diez-Perez and V. Mujica, *Small*, 2016, **13**, 1602519.
15 R. Naaman and D. H. Waldeck, *Annu. Rev. Phys. Chem.*, 2015, **66**, 263–281.
16 C. D. Aiello, J. M. Abendroth, M. Abbas, A. Afanasev, S. Agarwal, A. S. Banerjee, D. N. Beratan, J. N. Belling, B. Berche, A. Botana, J. R. Caram, G. L. Celardo, G. Cuniberti, A. Garcia-Etxarri, A. Dianat, I. Diez-Perez, Y. Q. Guo, R. Gutierrez, C. Herrmann, J. Hihath, S. Kale, P. Kurian, Y. C. Lai, T. H. Liu, A. Lopez, E. Medina, V. Mujica, R. Naaman, M. Noormandipour, J. L. Palma, Y. Paltiel, W. Petuskey, J. C. Ribeiro-Silva, J. J. Saenz, E. J. G. Santos, M. Solyanik-Gorgone, V. J. Sorger, D. M. Stemer, J. M. Ugalde, A. Valdes-Curiel, S. Varela, D. H. Waldeck, M. R. Wasielewski, P. S. Weiss, H. Zacharias and Q. H. Wang, *ACS Nano*, 2022, **16**, 4989–5035.
17 D. Z. Qi, A. Kenaan, D. X. Cui and J. Song, *Nano Energy*, 2018, **52**, 142–152.
18 H. Alpern, E. Katzir, S. Yochelis, N. Katz, Y. Paltiel and O. Millo, *New J. Phys.*, 2016, **18**, 113048.
19 G. Koplovitz, D. Primc, O. Ben Dor, S. Yochelis, D. Rotem, D. Porath and Y. Paltiel, *Adv. Mater.*, 2017, **29**, 1606748.
20 O. Ben Dor, S. Yochelis, A. Radko, K. Vankayala, E. Capua, A. Capua, S. H. Yang, L. T. Baczewski, S. S. P. Parkin, R. Naaman and Y. Paltiel, *Nat. Commun.*, 2017, **8**, 14567.
21 X. N. Sun, A. Bedoya-Pinto, Z. P. Mao, M. Gobbi, W. J. Yan, Y. L. Guo, A. Atxabal, R. Llopis, G. Yu, Y. Q. Liu, A. Chuvilin, F. Casanova and L. E. Hueso, *Adv. Mater.*, 2016, **28**, 2609–2615.
22 X. N. Sun, S. Velez, A. Atxabal, A. Bedoya-Pinto, S. Parui, X. W. Zhu, R. Llopis, F. Casanova and L. E. Hueso, *Science*, 2017, **357**, 677–680.
23 J. M. Abendroth, D. M. Stemer, B. P. Bloom, P. Roy, R. Naaman, D. H. Waldeck, P. S. Weiss and P. C. Mondal, *ACS Nano*, 2019, **13**, 4928–4946.
24 T. P. Fay and D. T. Limmer, *Nano Lett.*, 2021, **21**, 6696–6702.
25 O. Ben Dor, S. Yochelis, H. Ohldag and Y. Paltiel, *Chimia*, 2018, **72**, 379–383.
26 P. C. Mondal, P. Roy, D. Kim, E. E. Fullerton, H. Cohen and R. Naaman, *Nano Lett.*, 2016, **16**, 2806–2811.
27 H. Einati, D. Mishra, N. Friedman, M. Sheves and R. Naaman, *Nano Lett.*, 2015, **15**, 1052–1056.
28 J. Q. Ma, H. Z. Wang and D. H. Li, *Adv. Mater.*, 2021, **33**, 2008785.
29 G. K. Long, C. Y. Jiang, R. Sabatini, Z. Y. Yang, M. Y. Wei, L. N. Quan, Q. M. Liang, A. Rasmita, M. Askerka, G. Walters, X. W. Gong, J. Xing, X. L. Wen, R. Quintero-Bermudez, H. F. Yuan, G. C. Xing, X. R. Wang, D. T. Song, O. Voznyy, M. T. Zhang, S. Hoogland, W. B. Gao, Q. H. Xiong and E. H. Sargent, *Nat. Photonics*, 2018, **12**, 528–534.
30 S. Ma, J. Ahn and J. Moon, *Adv. Mater.*, 2021, **33**, 2005760.
31 W. Su and F. Yuan, *Sci. Bull.*, 2022, **67**(15), 1535–1538.
32 Y. Y. Dang, X. L. Liu, B. Q. Cao and X. T. Tao, *Matter*, 2021, **4**, 794–820.
33 H. P. Lu, J. Y. Wang, C. X. Xiao, X. Pan, X. H. Chen, R. Brunecky, J. J. Berry, K. Zhu, M. C. Beard and Z. V. Vardeny, *Sci. Adv.*, 2019, **5**, eaay0571.
34 Z. J. Huang, B. P. Bloom, X. J. Ni, Z. N. Georgieva, M. Marciesky, E. Vetter, F. Liu, D. H. Waldeck and D. L. Sun, *ACS Nano*, 2020, **14**, 10370–10375.
35 W. Y. Gao, H. Dong, N. Sun, L. F. Chao, W. Hui, Q. Wei, H. Li, Y. D. Xia, X. Y. Gao, G. C. Xing, Z. B. Wu, L. Song, P. Müller-Buschbaum, C. X. Ran and Y. H. Chen, *J. Energy Chem.*, 2022, **68**, 789–796.
36 D. H. Waldeck, R. Naaman and Y. Paltiel, *APL Mater.*, 2021, **9**, 040902.
37 F. Gao, P. C. Yuan, H. F. Ma, T. Xu, J. W. Zhu, K. X. Li, F. Yang and B. Yan, *EPL*, 2020, **132**, 15001.
38 R. Naaman and D. H. Waldeck, *J. Phys. Chem. Lett.*, 2012, **3**, 2178–2187.
39 K. Michaeli, V. Varade, R. Naaman and D. H. Waldeck, *J. Phys.: Condens. Matter*, 2017, **29**, 103002.
40 R. Naaman and D. H. Waldeck, *Annu. Rev. Phys. Chem.*, 2015, **66**, 263–281.
41 R. Naaman, *Isr. J. Chem.*, 2016, **56**, 1010–1015.
42 M. S. Gao and W. Qin, *Adv. Opt. Mater.*, 2021, **9**, 2101201.
43 R. Gutierrez, E. Diaz, R. Naaman and G. Cuniberti, *Phys. Rev. B: Condens. Matter Mater. Phys.*, 2012, **85**, 081404.
44 A. M. Guo and Q. F. Sun, *Phys. Rev. B: Condens. Matter Mater. Phys.*, 2012, **86**, 115441.
45 R. Gutierrez, E. Diaz, C. Gaul, T. Brumme, F. Dominguez-Adame and G. Cuniberti, *J. Phys. Chem. C*, 2013, **117**, 22276–22284.

46 E. Medina, L. A. Gonzalez-Arraga, D. Finkelstein-Shapiro, B. Berche and V. Mujica, *J. Chem. Phys.*, 2015, **142**, 194308.
47 S. Matityahu, Y. Utsumi, A. Aharony, O. Entin-Wohlman and C. A. Balseiro, *Phys. Rev. B*, 2016, **93**, 075407.
48 E. Medina, F. Lopez, M. A. Ratner and V. Mujica, *EPL*, 2012, **99**, 17006.
49 D. Nurenberg and H. Zacharias, *Phys. Chem. Chem. Phys.*, 2019, **21**, 3761–3770.
50 S. Alwan and Y. Dubi, *J. Am. Chem. Soc.*, 2021, **143**, 14235–14241.
51 J. Gersten, K. Kaasbjerg and A. Nitzan, *J. Chem. Phys.*, 2013, **139**, 114111.
52 R. Naaman, Y. Paltiel and D. H. Waldeck, *J. Phys. Chem. Lett.*, 2020, **11**, 3660–3666.
53 A. M. Garcia, G. Martinez and A. Ruiz-Carretero, *Front. Chem.*, 2021, **9**, 722727.
54 F. Evers, A. Aharony, N. Bar-Gill, O. Entin-Wohlman, P. Hedegard, O. Hod, P. Jelinek, G. Kamieniarz, M. Lemeshko, K. Michaeli, V. Mujica, R. Naaman, Y. Paltiel, S. Refaely-Abramson, O. Tal, J. Thijssen, M. Thoss, J. M. van Ruitenbeek, L. Venkataraman, D. H. Waldeck, B. H. Yan and L. Kronik, *Adv. Mater.*, 2022, **34**, 2106629.
55 S. Dalum and P. Hedegard, *Nano Lett.*, 2019, **19**, 5253–5359.
56 A. Kumar, E. Capua, M. K. Kesharwani, J. M. L. Martin, E. Sitbon, D. H. Waldeck and R. Naaman, *Proc. Natl. Acad. Sci. U. S. A.*, 2017, **114**, 2474–2478.
57 R. Naaman, Y. Paltiel and D. H. Waldeck, *Chimia*, 2018, **72**, 394–398.
58 J. Fransson, *J. Phys. Chem. Lett.*, 2019, **10**, 7126–7132.
59 J. Fransson, *Phys. Rev. B*, 2020, **102**, 235416.
60 J. Fransson, *Nano Lett.*, 2021, **21**, 3026–3032.
61 L. L. Zhang, Y. Y. Hao, W. Qin, S. J. Xie and F. Y. Qu, *Phys. Rev. B*, 2020, **102**, 214303.
62 C. Z. Wang, V. Mujica and Y. C. Lai, *Nano Lett.*, 2021, **21**, 10423–10430.
63 T. K. Das, F. Tassinari, R. Naaman and J. Fransson, *J. Phys. Chem. C*, 2022, **126**, 3257–3264.
64 Y. Shimamoto, Y. Matsushima, T. Hasegawa, Y. Kousaka, I. Proskurin, J. Kishine, A. S. Ovchinnikov, F. J. T. Goncalves and Y. Togawa, *Phys. Rev. Lett.*, 2022, **128**, 247203.
65 J. Fransson, *J. Phys. Chem. Lett.*, 2022, **13**, 808–814.
66 S. S. Chandran, Y. Wu, H. H. Teh, D. H. Waldeck and J. E. Subotnik, *J. Chem. Phys.*, 2022, **156**, 174113.
67 H. H. Teh, W. Dou and J. E. Subotnik, **https://arxiv.org/abs/2111.12815**.
68 M. Geyer, R. Gutierrez and G. Cuniberti, *J. Chem. Phys.*, 2020, **152**, 214105.
69 X. P. Li, J. Nan and X. C. Pan, *Phys. Rev. Lett.*, 2020, **125**, 263002.
70 T. Ritz, S. Adem and K. Schulten, *Biophys. J.*, 2000, **78**, 707–718.
71 R. Wiltschko and W. Wiltschko, *J. R. Soc., Interface*, 2019, **16**, 20190295.
72 C. T. Rodgers and P. J. Hore, *Proc. Natl. Acad. Sci. U. S. A.*, 2009, **106**, 353–360.
73 J. T. Luo and P. J. Hore, *New J. Phys.*, 2021, **23**, 043032.
74 T. P. Fay, *J. Phys. Chem. Lett.*, 2021, **12**, 1407–1412.
75 K. Michaeli, V. Varade, R. Naaman and D. H. Waldeck, *J. Phys.: Condens. Matter*, 2017, **29**, 103002.
76 K. Michaeli and R. Naaman, *J. Phys. Chem. C*, 2019, **123**, 17043–17048.
77 C. Vittmann, R. K. Kessing, J. Lim, S. F. Huelga and M. B. Plenio, *J. Phys. Chem. Lett.*, 2022, **13**, 1791–1796.
78 E. Diaz, P. Albares, P. G. Estevez, J. M. Cervero, C. Gaul, E. Diez and F. Dominguez-Adame, *New J. Phys.*, 2018, **20**, 043055.
79 S. Varela, B. Montanes, F. Lopez, B. Berche, B. Guillot, V. Mujica and E. Medina, *J. Chem. Phys.*, 2019, **151**, 125102.
80 J. D. Torres, R. Hidalgo-Sacoto, S. Varela and E. Medina, *Phys. Rev. B*, 2020, **102**, 035426.
81 Y. Dubi, *Chem. Sci.*, 2022, **13**, 10878–10883.
82 R. Naaman, C. Fontanesi and D. H. Waldeck, *Curr. Opin. Electrochem.*, 2019, **14**, 138–142.
83 I. Carmeli, V. Skakalova, R. Naaman and Z. Vager, *Angew. Chem., Int. Ed.*, 2002, **114**, 787–790.
84 V. Kiran, S. R. Cohen and R. Naaman, *J. Chem. Phys.*, 2017, **146**, 092302.
85 M. Kettner, B. Göhler, H. Zacharias, D. Mishra, V. Kiran, R. Naaman, C. Fontanesi, D. H. Waldeck, S. Sęk, J. Pawłowski and J. Juhaniewicz, *J. Phys. Chem. C*, 2015, **119**, 14542–14547.
86 Y. Z. Liu, J. W. Xiao, J. Koo and B. H. Yan, *Nat. Mater.*, 2021, **20**, 638–644.
87 Y. Wolf, Y. Z. Liu, J. W. Xiao, N. Park and B. H. Yan, *ACS Nano*, 2022, **16**, 18601–18607.
88 E. Z. B. Smolinsky, A. Neubauer, A. Kumar, S. Yochelis, E. Capua, R. Carmieli, Y. Paltiel, R. Naaman and K. Michaeli, *J. Phys. Chem. Lett.*, 2019, **10**, 1139–1145.
89 S. Mishra, A. K. Mondal, E. Z. B. Smolinsky, R. Naaman, K. Maeda, T. Nishimura, T. Taniguchi, T. Yoshida, K. Takayama and E. Yashima, *Angew. Chem., Int. Ed.*, 2020, **59**, 14671–14676.
90 V. V. Maslyuk, R. Gutierrez, A. Dianat, V. Mujica and G. Cuniberti, *J. Phys. Chem. Lett.*, 2018, **9**, 5453–5459.
91 A. Dianat, R. Gutierrez, H. Alpern, V. Mujica, A. Ziv, S. Yochelis, O. Millo, Y. Paltiel and G. Cuniberti, *Nano Lett.*, 2020, **20**, 7077–7086.
92 J. M. Matxain, J. M. Ugalde, V. Mujica, S. I. Allec, B. M. Wong and D. Casanova, *ChemPhotoChem*, 2019, **3**, 770–777.
93 M. S. Zollner, A. Saghatchi, V. Mujica and C. Herrmann, *J. Chem. Theory Comput.*, 2020, **16**, 7357–7371.
94 M. S. Zollner, S. Varela, E. Medina, V. Mujica and C. Herrmann, *J. Chem. Theory Comput.*, 2020, **16**, 2914–2929.
95 S. Mishra, A. Kumar, M. Venkatesan, L. Pigani, L. Pasquali and C. Fontanesi, *Small Methods*, 2020, **4**, 2000617.
96 Y. D. Xu, X. F. Han, Y. Xiao, Y. Wang and W. B. Mi, *Adv. Quantum Technol.*, 2022, 2200037.
97 T. J. Zwang, S. Hurlimann, M. G. Hill and J. K. Barton, *J. Am. Chem. Soc.*, 2016, **138**, 15551–15554.
98 Z. T. Xie, T. Z. Markus, S. R. Cohen, Z. Vager, R. Gutierrez and R. Naaman, *Nano Lett.*, 2011, **11**, 4652–4655.

99 P. C. Mondal, N. Kantor-Uriel, S. P. Mathew, F. Tassinari, C. Fontanesi and R. Naaman, *Adv. Mater.*, 2015, **27**, 1924–1927.
100 J. M. Abendroth, N. Nakatsuka, M. Ye, D. Kim, E. E. Fullertor, A. M. Andrews and P. S. Weiss, *ACS Nano*, 2017, **11**, 7516–7526.
101 M. Eckshtain-Levi, E. Capua, S. Refaely-Abramson, S. Sarkar, Y. Gavrilov, S. P. Mathew, Y. Paltiel, Y. Levy, L. Kronik and R. Naaman, *Nat. Commun.*, 2016, **7**, 10744.
102 Z. J. Huang, B. P. Bloom, X. J. Ni, Z. N. Georgieva, M. Marciesky, E. Vetter, F. Liu, D. H. Waldeck and D. L. Sun, *ACS Nano*, 2020, **14**, 10370–10375.
103 K. S. Kumar, N. Kantor-Uriel, S. P. Mathew, R. Guliamov and R. Naaman, *Phys. Chem. Chem. Phys.*, 2013, **15**, 18357–18362.
104 B. P. Bloom, R. Liu, P. Zhang, S. Ghosh, R. Naaman, D. N. Beratan and D. H. Waldeck, *Acc. Chem. Res.*, 2018, **51**, 2565–2573.
105 W. Y. Zhang, K. Banerjee-Ghosh, F. Tassinari and R. Naaman, *ACS Energy Lett.*, 2018, **3**, 2308–2313.
106 A. A. Ageeva, E. A. Khramtsova, I. M. Magin, P. A. Purtov, M. A. Miranda and T. V. Leshina, *Chem. – Eur. J.*, 2018, **24**, 18587–18600.
107 A. A. Ageeva, E. A. Khramtsova, I. M. Magin, D. A. Rychkov, P. A. Purtov, M. A. Miranda and T. V. Leshina, *Chem. – Eur. J.*, 2018, **24**, 3882–3892.
108 I. Carmeli, V. Skakalova, R. Naaman and Z. Vager, *Angew. Chem., Int. Ed.*, 2002, **41**, 761–764.
109 C. Nogues, S. R. Cohen, S. S. Daube and R. Naaman, *Phys. Chem. Chem. Phys.*, 2004, **6**, 4459–4466.
110 S. G. Ray, S. S. Daube, G. Leitus, Z. Vager and R. Naaman, *Phys. Rev. Lett.*, 2006, **96**, 036101.
111 A. M. Guo and Q. F. Sun, *Phys. Rev. Lett.*, 2012, **108**, 218102.
112 F. Zhao, Q. Q. Meng and Y. Chen, *Commun. Theor. Phys.*, 2014, **61**, 755–758.
113 D. N. Beratan, R. Naaman and D. H. Waldeck, *Curr. Opin. Electrochem.*, 2017, **4**, 175–181.
114 S. V. Salazar, V. Mujica and E. Medina, *Chimia*, 2018, **72**, 411–417.
115 S. Mishra, A. K. Mondal, S. Pal, T. K. Das, E. Z. B. Smolinsky, G. Siligardi and R. Naaman, *J. Phys. Chem. C*, 2020, **124**, 10776–10782.
116 G. F. Du, H. H. Fu and R. Q. Wu, *Phys. Rev. B*, 2020, **102**, 035431.
117 P. V. Möllers, S. Ulku, D. Jayarathna, F. Tassinari, D. Nurenberg, R. Naaman, C. Achim and H. Zacharias, *Chirality*, 2021, **33**, 93–102.
118 K. M. Alam and K. S. Pramani, *Nanoscale*, 2017, **9**, 5155–5163.
119 M. W. Rahman, S. Firouzeh, V. Mujica and S. Pramanik, *ACS Nano*, 2020, **14**, 3389–3396.
120 M. W. Rahman, S. Firouzeh and S. Pramanik, *Nanotechnology*, 2021, **32**, 455001.
121 G. Bonnet, O. Krichevsky and A. Libchaber, *Proc. Natl. Acad. Sci. U. S. A.*, 1998, **95**, 8602–8606.
122 N. L. Goddard, G. Bonnet, O. Krichevsky and A. Libchaber, *Phys. Rev. Lett.*, 2000, **85**, 2400–2403.
123 S. Tyagi, D. P. Bratu and F. R. Kramer, *Nat. Biotechnol.*, 1998, **16**, 49–53.
124 P. J. Hu, S. X. Wang, X. H. Gao, Y. Y. Zhang, T. F. Fang, A. M. Guo and Q. F. Sun, *Phys. Rev. B*, 2020, **102**, 195406.
125 A. B. Hammam, B. Shylee, M. Tzuriel, V. Daniel, Y. Shira, S. Oded and P. Yossi, *Biomacromolecules*, 2022, **23**, 2098–2105.
126 D. Mishra, T. Z. Markus, R. Naaman, M. Kettner, B. Gohler, H. Zacharias, N. Friedman, M. Sheves and C. Fontanesi, *Proc. Natl. Acad. Sci. U. S. A.*, 2013, **110**, 14872–14876.
127 I. Carmeli, K. S. Kumar, O. Heifler, C. Carmeli and R. Naaman, *Angew. Chem., Int. Ed.*, 2014, **53**, 8953–8958.
128 T. R. Pan, A. M. Guo and Q. F. Sun, *Phys. Rev. B: Condens. Matter Mater. Phys.*, 2015, **92**, 115418.
129 Y. T. Sang, S. Mishra, F. Tassinari, S. K. Karuppannan, R. Carmieli, R. D. Teo, A. Migliore, D. N. Beratan, H. B. Gray, I. Pecht, J. Fransson, D. H. Waldeck and R. Naaman, *J. Phys. Chem. C*, 2021, **125**, 9875–9883.
130 W. Y. Zhang, J. Li, G. X. Lu, H. M. Guan and L. Y. Hao, *Chem. Commun.*, 2019, **55**, 13390–13393.
131 G. Bullard, F. Tassinari, C. H. Ko, A. K. Mondal, R. Wang, S. Mishra, R. Naaman and M. J. Therien, *J. Am. Chem. Soc.*, 2019, **141**, 14707–14711.
132 K. Banerjee-Ghosh, O. Ben Dor, F. Tassinari, E. Capua, S. Yochelis, A. Capua, S. H. Yang, S. S. P. Parkin, S. Sarkar, L. Kronik, L. T. Baczewski, R. Naaman and Y. Paltiel, *Science*, 2018, **360**, 1331–1334.
133 S. Ghosh, S. Mishra, E. Avigad, B. P. Bloom, L. T. Baczewski, S. Yochelis, Y. Paltiel, R. Naaman and D. H. Waldeck, *J. Phys. Chem. Lett.*, 2020, **11**, 1550–1557.
134 H. Al-Bustami, G. Koplovitz, D. Primc, S. Yochelis, E. Capua, D. Porath, R. Naaman and Y. Paltiel, *Small*, 2018, **14**, 1801249.
135 H. Al-Bustami, B. P. Bloom, A. Ziv, S. Goldring, S. Yochelis, R. Naaman, D. H. Waldeck and Y. Paltiel, *Nano Lett.*, 2020, **20**, 8675–8681.
136 F. Blumenschein, M. Tamski, C. Roussel, E. Z. B. Smolinsky, F. Tassinari, R. Naaman and J. P. Ansermet, *Phys. Chem. Chem. Phys.*, 2020, **22**, 997–1002.
137 C. Fontanesi, *Curr. Opin. Electrochem.*, 2018, **7**, 36–41.
138 W. Y. Zhang, H. M. Guan, C. Y. Kuang, W. Wang, Y. F. Hu and X. L. Yang, *Mater. Lett.*, 2022, **308**, 131130.
139 R. Naaman, Y. Paltiel and D. H. Waldeck, *Nat. Rev. Chem.*, 2019, **3**, 250–260.
140 R. Naaman, Y. Paltiel and D. H. Waldeck, *Annu. Rev. Biophys.*, 2022, **51**, 99–114.
141 S. Mishra, S. Pirbadian, A. K. Mondal, M. Y. El-Naggar and R. Naaman, *J. Am. Chem. Soc.*, 2019, **141**, 19198–19202.
142 C. Xie, *Innovation*, 2022, **3**, 100229.
143 R. Naaman and D. H. Waldeck, *J. Phys. Chem. Lett.*, 2012, **3**, 2178–2187.
144 F. Tassinari, D. Amsallem, B. P. Bloom, Y. Y. Lu, A. Bedi, D. H. Waldeck, O. Gidron and R. Naaman, *J. Phys. Chem. C*, 2020, **124**, 20974–20980.
145 D. G. Billing and A. Lemmerer, *Acta Crystallogr., Sect. E: Struct. Rep. Online*, 2003, **59**, M381–M383.

146 Z. G. Yu, *J. Phys. Chem. Lett.*, 2020, **11**, 8638–8646.
147 T. L. Feng, Z. Y. Wang, Z. X. Zhang, J. Xue and H. P. Lu, *Nanoscale*, 2021, **13**, 18925.
148 F. F. Gao, X. Li, Y. Qin, Z. G. Li, T. M. Guo, Z. Z. Zhang, G. D. Su, C. Y. Jiang, M. Azeem, W. Li, X. Wu and X. H. Bu, *Adv. Opt. Mater.*, 2021, **9**, 2100003.
149 S. D. Elliott, M. P. Moloney and Y. K. Gun'ko, *Nano Lett.*, 2008, **8**, 2452–2457.
150 T. Nakashima, Y. Kobayashi and T. Kawai, *J. Am. Chem. Soc.*, 2009, **131**, 10342–10343.
151 T. He, J. Li, X. Li, C. Ren, Y. Luo, F. Zhao, R. Chen, X. Lin and J. Zhang, *Appl. Phys. Lett.*, 2017, **111**, 151102.
152 A. Ben-Moshe, A. O. Govorov and G. Markovich, *Angew. Chem., Int. Ed.*, 2013, **125**, 1313–1317.
153 J. Ahn, E. Lee, J. Tan, W. Yang, B. Kim and J. Moon, *Mater. Horiz.*, 2017, **4**, 851–856.
154 H. E. Lee, H. Y. Ahn, J. Mun, Y. Y. Lee, M. Kim, N. H. Cho, K. Chang, W. S. Kim, J. Rho and K. T. Nam, *Nature*, 2018, **556**, 360–365.
155 Y. Shi, P. Duan, S. Huo, Y. Li and M. Liu, *Adv. Mater.*, 2018, **30**, 1705011.
156 A. O. Govorov, Z. Fan, P. Hernandez, J. M. Slocik and R. R. Naik, *Nano Lett.*, 2010, **10**, 1374–1382.
157 Y. Zhang, M. Sun, N. Zhou, B. Huang and H. Zhou, *J. Phys. Chem. Lett.*, 2020, **11**, 7610–7616.
158 S. Ma, Y. K. Jung, J. Ahn, J. Kyhm, J. Tan, H. Lee, G. Jang, C. U. Lee, A. Walsh and J. Moon, *Nat. Commun.*, 2022, **13**, 3259.
159 Z. Wang, Z. Zhang, H. H. Y. Sung, L. D. Williams and H. P. Lu, *Eur. J. Inorg. Chem.*, 2022, e202200275.
160 C. Zhang, D. Sun, C. X. Sheng, Y. X. Zhai, K. Mielczarek, A. Zakhidov and Z. V. Vardeny, *Nat. Phys.*, 2015, **11**, 428–435.
161 D. G. Billing and A. Lemmerer, *CrystEngComm*, 2006, **8**, 686–695.
162 J. Q. Ma, C. Fang, C. Chen, L. Jin, J. Q. Wang, S. Wang, J. Tang and D. H. Li, *ACS Nano*, 2019, **13**, 3659–3665.
163 Y. H. Kim, Y. X. Zhai, H. P. Lu, X. Pan, C. X. Xiao, E. A. Gaulding, S. P. Harvey, J. J. Berry, Z. V. Vardeny, J. M. Luther and M. C. Beard, *Science*, 2021, **371**, 1129–1133.
164 G. Long, G. Adamo, J. Tian, M. Klein, H. N. S. Krishnamoorthy, E. Feltri, H. Wang and C. Soci, *Nat. Commun.*, 2022, **13**, 1551.
165 C. Ye, J. Jiang, S. Zou, W. Mi and Y. Xiao, *J. Am. Chem. Soc.*, 2022, **144**, 9707–9714.
166 B. Li, Y. Yu, M. Xin, J. Xu, T. Zhao, H. Kang, G. Xing, P. Zhao, T. Zhang and S. Jiang, *Nanoscale*, 2023, **15**, 1595–1601.
167 K. Kim, E. Vetter, L. Yan, C. Yang, Z. Wang, R. Sun, Y. Yang, A. H. Comstock, X. Li, J. Zhou, L. Zhang, W. You, D. Sun and J. Liu, *Nat. Mater.*, 2023, 1–7.
168 H. P. Lu, C. X. Xiao, R. Y. Song, T. Y. Li, A. E. Maughan, A. Levin, R. Brunecky, J. J. Berry, D. B. Mitzi, V. Blum and M. C. Beard, *J. Am. Chem. Soc.*, 2020, **142**, 13030–13040.
169 Y. Lu, Q. Wang, R. Y. Chen, L. L. Qiao, F. X. Zhou, X. Yang, D. Wang, H. Cao, W. L. He, F. Pan, Z. Yang and C. Song, *Adv. Funct. Mater.*, 2021, **31**, 2104605.
170 Y. Lu, Q. Wang, R. L. He, F. X. Zhou, X. Yang, D. Wang, H. Cao, W. L. He, F. Pan, Z. Yang and C. Song, *Angew. Chem., Int. Ed.*, 2021, **60**, 23578–23583.
171 Q. Wang, Y. Lu, R. L. He, R. Chen, L. Qiao, F. Pan, Z. Yang and C. Song, *Small Methods*, 2022, **6**, 2201048.
172 Q. Wei, Q. Zhang, L. Xiang, S. Zhang, J. Liu, X. Yang, Y. Ke and Z. Ning, *J. Phys. Chem. Lett.*, 2021, **12**, 6492–6498.
173 K. Leng, R. Li, S. P. Lau and K. P. Loh, *Trends Chem.*, 2021, **3**, 716–732.
174 Y. H. Kim, R. Y. Song, J. Hao, Y. X. Zhai, L. Yan, T. Moot, A. F. Palmstrom, R. Brunecky, W. You, J. J. Berry, J. L. Blackburn, M. C. Beard, V. Blum and J. M. Luther, *Adv. Funct. Mater.*, 2022, **32**, 2200454.
175 R. Torres-Cavanillas, G. Escorcia-Ariza, I. Brotons-Alcazar, R. Sanchis-Gual, P. C. Mondal, L. E. Rosaleny, S. Gimenez-Santamarina, M. Sessolo, M. Galbiati, S. Tatay, A. Gaita-Arino, A. Forment-Aliaga and S. Cardona-Serra, *J. Am. Chem. Soc.*, 2020, **142**, 17572–17580.
176 U. Huizi-Rayo, J. Gutierrez, J. M. Seco, V. Mujica, I. Diez-Perez, J. M. Ugalde, A. Tercjak, J. Cepeda and E. San Sebastian, *Nano Lett.*, 2020, **20**, 8476–8482.
177 C. C. Wang, A. M. Guo, Q. F. Sun and Y. Yan, *J. Phys. Chem. Lett.*, 2021, **12**, 10262–10269.
178 N. Goren, T. K. Das, N. Brown, S. Gilead, S. Yochelis, E. Gazit, R. Naaman and Y. Paltiel, *Nano Lett.*, 2021, **21**, 8657–8663.
179 Q. Qian, H. Y. Ren, J. Y. Zhou, Z. Wan, J. X. Zhou, X. X. Yan, J. Cai, P. Q. Wang, B. L. Li, Z. Sofer, B. Li, X. D. Duan, X. Q. Pan, Y. Huang and X. F. Duan, *Nature*, 2022, **606**, 902–908.
180 Z. Y. Bian, K. Kato, T. Ogoshi, Z. Cui, B. S. Sa, Y. Tsutsui, S. Seki and M. Suda, *Adv. Sci.*, 2022, **9**, 2201063.
181 L. Addadi and S. Weiner, *Nature*, 2001, **411**, 753–755.
182 Y. Nabei, D. Hirobe, Y. Shimamoto, K. Shiota, A. Inui, Y. Kousaka, Y. Togawa and H. M. Yamamoto, *Appl. Phys. Lett.*, 2020, **117**, 052408.
183 A. Inui, R. Aoki, Y. Nishiue, K. Shiota, Y. Kousaka, H. Shishido, D. Hirobe, M. Suda, J. Ohe, J. Kishine, H. M. Yamamoto and Y. Togawa, *Phys. Rev. Lett.*, 2020, **124**, 166602.
184 H. Shishido, R. Sakai, Y. Hosaka and Y. Togawa, *Appl. Phys. Lett.*, 2021, **119**, 182403.
185 K. Shiota, A. Inui, Y. Hosaka, R. Amano, Y. Onuki, M. Hedo, T. Nakama, D. Hirobe, J. Ohe, J. Kishine, H. M. Yamamoto, H. Shishido and Y. Togawa, *Phys. Rev. Lett.*, 2021, **127**, 126602.
186 T. Furukawa, Y. Shimokawa, K. Kobayashi and T. Itou, *Nat. Commun.*, 2017, **8**, 954.
187 T. Furukawa, Y. Watanabe, N. Ogasawara, K. Kobayashi and T. Itou, *Phys. Rev. Res.*, 2021, **3**, 023111.
188 H. Chen, W. Wu, J. Zhu, Z. Yang, W. Gong, W. Gao, S. A. Yang and L. Zhang, *Nano Lett.*, 2022, **22**, 1688–1693.
189 J. R. Swierk, D. D. Mendez-Hernandez, N. S. McCool, P. Liddell, Y. Terazono, I. Pahk, J. J. Tomlin, N. V. Oster, T. A. Moore, A. L. Moore, D. Gust and T. E. Mallouk, *Proc. Natl. Acad. Sci. U. S. A.*, 2015, **112**, 1681–1686.

190 B. P. Bloom, Y. Lu, T. Metzger, S. Yochelis, Y. Paltiel, C. Fontanesi, S. Mishra, F. Tassinari, R. Naaman and D. H. Waldeck, *Phys. Chem. Chem. Phys.*, 2020, **22**, 21570–21582.
191 H. M. Kothari, E. A. Kulp, S. Boonsalee, M. P. Nikiforov, E. W. Bohannan, P. Poizot, S. Nakanishi and J. A. Switzer, *Chem. Mater.*, 2004, **16**, 4232–4244.
192 R. Widmer, F. Haug, P. Ruffieux, O. Gröning, M. Bielmann, P. Gröning and R. Fasel, *J. Am. Chem. Soc.*, 2006, **128**, 14103–14108.
193 K. B. Ghosh, W. Y. Zhang, F. Tassinari, Y. Mastai, O. Lidor-Shaley, R. Naaman, P. Mollers, D. Nurenberg, H. Zacharias, J. Wei, E. Wierzbinski and D. H. Waldeck, *J. Phys. Chem. C*, 2019, **123**, 3024–3031.
194 W. Y. Zhang, W. Wang, Y. F. Hu, H. M. Guan, X. L. Yang and L. Y. Hao, *Int. J. Hydrogen Energy*, 2021, **46**, 8922–8931.
195 S. Ghosh, B. P. Bloom, Y. Lu, D. Lamont and D. H. Waldeck, *J. Phys. Chem. C*, 2020, **124**, 22610–22618.
196 T. Bai, J. Ai, Y. Y. Duan, L. Han and S. N. Che, *Small*, 2022, **18**, 2104509.
197 T. Bai, J. Ai, L. Liao, J. Luo, C. Song, Y. Duan, L. Han and S. Che, *Angew. Chem., Int. Ed.*, 2021, **60**, 9421–9426.
198 E. P. D'yachkov and P. N. D'yachkov, *J. Phys. Chem. C*, 2019, **123**, 26005–26010.
199 D. A. Hoff and L. G. C. Rego, *Nano Lett.*, 2021, **21**, 8190–8196.
200 Z. Liu, J. Ai, T. Bai, Y. Fang, K. Ding, Y. Duan, L. Han and S. Che, *Chem*, 2022, **8**, 186–196.
201 M. Gazzotti, S. Arnaboldi, S. Grecchi, R. Giovanardi, M. Cannio, L. Pasquali, A. Giacomino, O. Abollino and C. Fontanesi, *Electrochim. Acta*, 2018, **286**, 271–278.
202 R. Naaman, Y. Paltiel and D. H. Waldeck, *Acc. Chem. Res.*, 2020, **53**, 2659–2667.
203 B. P. Bloom, A. R. Waldeck and D. H. Waldeck, *Proc. Natl. Acad. Sci. U. S. A.*, 2022, **119**, e2210505119.
204 T. H. Liu, X. L. Wang, H. L. Wang, G. Shi, F. Gao, H. L. Feng, H. Y. Deng, L. Q. Hu, E. Lochner, P. Schlottmann, S. von Molnar, Y. Q. Li, J. H. Zhao and P. Xiong, *ACS Nano*, 2020, **14**, 15983–15991.
205 A. Chiesa, M. Chizzini, E. Garlatti, E. Salvadori, F. Tacchino, P. Santini, I. Tavernelli, R. Bittl, M. Chiesa, R. Sessoli and S. Carretta, *J. Phys. Chem. Lett.*, 2021, **12**, 6341–6347.
206 D. H. Waldeck, R. Naaman and Y. Paltiel, *APL Mater.*, 2021, **9**, 040902.
207 A. Forment-Aliaga and A. Gaita-Ariñoa, *J. Appl. Phys.*, 2022, **132**, 180901.
208 K. H. Huisman and J. M. Thijssen, *J. Phys. Chem. C*, 2021, **125**, 23364–23369.
209 K. Kondou, M. Shiga, S. Sakamoto, H. Inuzuka, A. Nihonyanagi, F. Araoka, M. Kobayashi, S. Miwa, D. Miyajima and Y. Otani, *J. Am. Chem. Soc.*, 2022, **144**, 7302–7307.
210 Z. X. Shang, T. H. Liu, Q. Q. Yang, S. N. Cui, K. L. Xu, Y. Zhang, J. X. Deng, T. R. Zhai and X. L. Wang, *Small*, 2022, 2203015.
211 V. Kiran, S. P. Mathew, S. R. Cohen, I. H. Delgado, J. Lacour and R. Naaman, *Adv. Mater.*, 2016, **28**, 1957–1962.
212 A. Ghazaryan, Y. Paltiel and M. Lemeshko, *J. Phys. Chem. C*, 2020, **124**, 11716–11721.
213 H. Watanabe, K. Hoshi and J. Ohe, *Phys. Rev. B*, 2016, **94**, 125143.
214 T. H. Kim, S. H. Han and B. K. Cho, *Commun. Phys.*, 2019, **2**, 41.
215 S. Yang, R. Naaman, Y. Paltiel and S. S. P. Parkin, *Nat. Rev. Phys.*, 2021, **3**, 328–343.